

Loopholes in Z' searches at the LHC: exploring supersymmetric and leptophobic scenarios

Jack Y. Araz^a, Gennaro Corcella^b, Mariana Frank^a and Benjamin Fuks^{c,d,e}

^a*Department of Physics, Concordia University*

7141 Sherbrooke St. West, Montreal, QC, Canada H4B 1R6

^b*INFN, Laboratori Nazionali di Frascati,*

Via E. Fermi 40, I-00044 Frascati (RM), Italy

^c*Sorbonne Universités, Université Pierre et Marie Curie*

(Paris 06), UMR 7589, LPTHE, F-75005 Paris, France

^d*CNRS, UMR 7589, LPTHE,*

F-75005, Paris, France

^e*Institut Universitaire de France,*

103 boulevard Saint-Michel, 75005 Paris, France

E-mail: jack.araz@concordia.ca, gennaro.corcella@lnf.infn.it,
mariana.frank@concordia.ca, fuks@lpthe.jussieu.fr

ABSTRACT: Searching for heavy vector bosons Z' , predicted in models inspired by Grand Unification Theories, is among the challenging objectives of the LHC. The ATLAS and CMS collaborations have looked for Z' bosons assuming that they can decay only into Standard Model channels, and have set exclusion limits by investigating dilepton, dijet and to a smaller extent top-antitop final states. In this work we explore possible loopholes in these Z' searches by studying supersymmetric as well as leptophobic scenarios. We demonstrate the existence of realizations in which the Z' boson automatically evades the typical bounds derived from the analyses of the Drell-Yan invariant-mass spectrum. Dileptonic final states can in contrast only originate from supersymmetric Z' decays and are thus accompanied by additional effects. This feature is analyzed in the context of judiciously chosen benchmark configurations, for which visible signals could be expected in future LHC data with a $4\sigma - 7\sigma$ significance. Our results should hence motivate an extension of the current Z' search program to account for supersymmetric and leptophobic models.

KEYWORDS: heavy neutral gauge boson, supersymmetry, UMSSM, LHC

Contents

1	Introduction	1
2	Z' bosons in $U(1)'$ supersymmetric models	3
2.1	Theoretical framework	3
2.2	Parameter-space scan and constraints	7
3	Supersymmetric Z' Phenomenology	10
3.1	Scenarios With High-Scale Boundary Conditions	10
3.2	Scenarios with Low-Scale Boundary Conditions	14
4	Leptophobic Z' Scenarios in UMSSM Models	16
5	Summary and Conclusions	26

1 Introduction

Although the discovery of the Higgs boson at the LHC has allowed for the completion of the particle spectrum of the Standard Model (SM), the issue of its extension still stands. Despite the experimental success in predicting most data observed so far, the SM indeed exhibits several limitations and shortcomings that motivate the study of beyond the Standard Model theories. Among those, supersymmetry, and in particular its minimal incarnation known as the Minimal Supersymmetric Standard Model (MSSM), is one of the most appealing options. Unifying internal and external symmetries, supersymmetry provides a natural solution to the long-standing hierarchy problem allows for gauge-coupling unification at high energies and predicts a stable particle that could address the problematics of dark matter. Despite these numerous motivations, no compelling evidence for supersymmetry has been found and the MSSM starts to be heavily constrained. Moreover, the MSSM suffers from severe fine-tuning issues related to the discovery of an SM-like Higgs boson, as well as the lack of any satisfactory explanation for the magnitude of the supersymmetric bilinear Higgs mass parameter μ that must unnaturally be of the order of the electroweak symmetry breaking scale.

As a consequence, arguments have been raised in favor of extending the MSSM superfield content by at least one singlet chiral superfield. Its scalar component can induce both supersymmetry breaking and dynamical generation of the μ term by getting a non-vanishing vacuum expectation value at the minimum of the scalar potential [1–5]. Such singlet superfields also appear under supersymmetric scenarios where the Standard Model gauge group is extended, the scalar singlet yielding the breaking of the additional gauge symmetry [6, 7]. This setup is furthermore motivated in a grand-unified scheme where a restricted set of

high-dimensional representations are used to encompass all MSSM supermultiplets, and where all gauge couplings unify. In this context, the necessity of using representations of the unified gauge group automatically leads to the introduction of right-handed neutrino superfields, which consequently provides a solution for neutrino-mass generation, as well as vector-like fermions.

Among all Grand Unification Theories (GUT), those based on gauge groups of rank 6, named E_6 , have been extensively discussed as interesting possibilities [7–9]. In particular, the breaking pattern of E_6 to the electroweak symmetry results in the appearance of extra $U(1)'$ symmetries. From a bottom-up perspective, extending the MSSM with the introduction of an extra $U(1)'$ gauge group has numerous advantages, namely forbidding a too rapid proton decay without introducing an *ad hoc* discrete R -parity symmetry and making all field masses stable with respect to quantum corrections. Moreover, it is always possible to choose the $U(1)'$ field charges to ensure anomaly cancellation and gauge-coupling unification. Besides, the $U(1)'$ models do not suffer from the presence of cosmological domain walls, unlike theories like the Next-to-Minimal Supersymmetric Standard Model [10, 11].

While the spectrum of $U(1)'$ supersymmetric (UMSSM) models is altered from that of the MSSM, the most secure prediction emerging from the extended gauge symmetry consists of the existence of a novel neutral Z' boson, like in non-supersymmetric $U(1)'$ extensions of the SM. This makes the Z' boson a prime target for the LHC physics program, as the proof of its existence would constitute a promising indicator of a more general gauge structure. Any gauge group of rank greater than four (any group larger than $SU(5)$) indeed leads to the appearance of at least one extra neutral gauge boson. All current Z' analyses at the LHC are however guided by non-supersymmetric considerations in which the Z' boson only decays into SM particles [12–16]. Besides E_6 -inspired Z' , the experimental collaborations have also explored the so-called Sequential Standard Model (SSM), the simplest extension of the Standard Model, wherein Z' and possible W' bosons have the same couplings to fermions as the Z and W . This model is not theoretically motivated, but it is often used as a benchmark for the analyses, since the production cross section in the SSM just depends on the extra boson masses.

Along these lines, the ATLAS and CMS collaborations have searched for Z' bosons by investigating dilepton and dijet final states. In detail, by using high-mass dilepton data at 13 TeV, the ATLAS collaboration [17] set the mass exclusion limits $M_{Z'} > 4.5$ TeV in the SSM and $M_{Z'} > 3.8$ – 4.1 TeV in $U(1)'$ models, whereas CMS obtained $M_{Z'} > 4.0$ TeV (SSM) and $M_{Z'} > 3.5$ TeV (GUT-inspired models) [18]. For dijets, the limits are much milder and read $M_{Z'} > 2.1$ – 2.9 TeV (ATLAS) [19] and $M_{Z'} > 2.7$ TeV (CMS) [20].

In a UMSSM framework, the inclusion of the supersymmetric decay modes of the Z' bosons may nonetheless change these conclusions [21–26]. Above all, the opening of new decay channels lowers the branching ratios into SM final states and therefore the Z' mass exclusion limits. In fact, Ref. [27] found an impact of about 200 GeV on the mass exclusion limits by comparing the 8 TeV ATLAS and CMS data on high-mass dileptons with UMSSM predictions for a benchmark point of the parameter space. Furthermore, in the UMSSM, a leptophobic Z' can yield the production of dilepton final states only through cascade decays into intermediate electroweakinos, which contrasts with the leptophobic

non-supersymmetric case where this is simply not allowed [28]. The bounds on the Z' -boson mass and production cross section derived from the above-mentioned searches should then be revisited when more general theoretical contexts like the UMSSM or leptophobia are considered.

On different grounds, the hadronic environment at the LHC is so complex that new physics searches always rely on some simplifying assumptions in the form of the potential signals. For instance, most supersymmetry searches have been designed from the idea on how the MSSM could manifest itself in a typical LHC detector: they may hence be not suitable for given non-minimal supersymmetric realizations. In the UMSSM framework, which we focus on in this work, we consider Z' -boson signals that can potentially differ from the non-supersymmetric case. We restrict our analysis to leptonic Z' decay modes that are easier to explore, even if the expected signals are plagued by larger SM backgrounds. We additionally focus on UMSSM realizations in which the Z' boson is leptophobic, but where it could give rise to leptonic signatures via supersymmetric cascade decays into leptons and missing energy. This therefore offers an alternative opportunity to find both an extra gauge boson and supersymmetry from the study of the decays of a resonantly produced colorless particle. This is one of the scenarios that we wish to investigate in this work, after imposing the most up-to-date constraints on the model. We hence aim at providing a clear roadmap for the discovery of unconventional leptophobic Z' bosons, such as those that could arise in UMSSM scenarios and that escape detection when only considering standard LHC searches for extra gauge bosons.

Our work is organized as follows. In Section 2, we briefly introduce $U(1)'$ supersymmetric models as when the gauge symmetry is designed as emerging from the breaking of an extended E_6 symmetry at the grand unification scale. We pay a particular attention to the mass, mixing patterns and interactions of the extra neutral gauge boson and show under what conditions it could be made leptophobic. We finally set up the parameter-space region to be scanned over and proceed to its exploration in Section 3, focusing on two different way to impose boundary conditions. In Section 4, we concentrate on scenarios where the Z' boson does not directly decay into leptons and study its phenomenology at colliders, highlighting a preferred selection strategy that could lead to its discovery. We summarize our results and conclude in Section 5.

2 Z' bosons in $U(1)'$ supersymmetric models

2.1 Theoretical framework

There are different ways to implement a $U(1)'$ extension in the MSSM: one of the most commonly used parameterizations is inspired by grand-unified models, based on a rank-6 group E_6 , where the symmetry-breaking scheme proceeds via multiple steps,

$$\begin{aligned} E_6 &\rightarrow SO(10) \otimes U(1)_\psi \rightarrow SU(5) \otimes U(1)_X \otimes U(1)_\psi \\ &\rightarrow SU(3)_C \otimes SU(2)_L \otimes U(1)_Y \otimes U(1)' . \end{aligned} \tag{2.1}$$

Model	$U(1)'_\chi$	$U(1)'_\psi$	$U(1)'_\eta$	$U(1)'_S$	$U(1)'_I$	$U(1)'_N$
θ_{E_6}	-0.5π	0	-0.79π	-0.37π	0.71π	-0.08π

Table 1. Mixing angle θ_{E_6} for the most popular $U(1)'$ models. The value of θ_{E_6} is imposed to lie in the $[-\pi, \pi]$ range.

	$2\sqrt{10}Q'_\chi$	$2\sqrt{6}Q'_\psi$	$2\sqrt{15}Q'_\eta$	$2\sqrt{15}Q'_S$	$2Q'_I$	$2\sqrt{10}Q'_N$
Q, U, E	-1	1	-2	-1/2	0	1
L, D	3	1	1	4	-1	2
N	-5	1	-5	-5	1	0
H_u	2	-2	4	1	0	2
H_d	-2	-2	1	-7/2	1	-3
S	0	4	-5	5/2	-1	5

Table 2. $U(1)'$ charges of the UMSSM quark (Q, D, U), lepton (L, E, N) and Higgs (H_u, H_d, S) supermultiplets for commonly studied anomaly-free $U(1)'$ groups that arise from the breaking of an E_6 symmetry.

The $U(1)'$ symmetry that survives at the electroweak scale is taken as a linear combination of $U(1)_\chi$ and $U(1)_\psi$,

$$U(1)' = \cos \theta_{E_6} U(1)_\psi - \sin \theta_{E_6} U(1)_\chi, \quad (2.2)$$

where we have introduced the E_6 mixing angle θ_{E_6} . The neutral vector bosons associated with the $U(1)_\psi$ and $U(1)_\chi$ gauge groups are called the Z'_ψ and Z'_χ bosons, while a generic Z' is given by the mixing of these Z'_ψ and Z'_χ states, as in Eq. (2.2).

Different $U(1)'$ models can be classified according to the sole value of the θ_{E_6} mixing angle, and the charges Q' of the supermultiplets are fixed to ensure the theory to be anomaly-free. Six popular setups are summarized in Table 1, with the corresponding Q' charges listed in Table 2. In the notations of this last table, Q and L denote the left-handed weak doublets of quark and lepton fields, H_u and H_d the two weak doublets of Higgs fields, U and D the right-handed weak singlets of up-type and down-type quarks, E and N the right-handed weak singlets of charged leptons and neutrinos, and S a scalar singlet. In the case of supersymmetric extensions of the Standard Model, such as the MSSM, all fields in Table 2 must actually be understood as superfields containing also the supersymmetric partners of the fermions and Higgs bosons. In principle, the matter sector of E_6 should also feature vector-like exotic (s)quarks Q_D and \bar{Q}_D which have the same $U(1)'$ charges as the H_u and H_d fields, respectively [8]. In the following, we assume that these exotic states are too heavy to be relevant at LHC energies and neglect them in our phenomenological analysis¹.

¹Due to the requirement of the $SU(3)_c - SU(3)_c - U(1)'$ anomaly cancellation, these exotic quarks have

The Higgs supermultiplet content (H_u , H_d and S) is large enough to allow both for the breaking of $U(1)'$ via the scalar singlet field s , and of the electroweak symmetry through the neutral components of the scalar Higgs doublets h_u and h_d . All electrically-neutral Higgs fields indeed get non-vanishing vacuum expectation values at the minimum of the potential and carry non-trivial $U(1)'$ charges.

In the grand unified framework, the field content is organized into vector representations (**27**) of the E_6 group; the latter further branches as $\mathbf{27} = \mathbf{16} \oplus \bar{\mathbf{10}} \oplus \mathbf{1}$ into the irreducible representations of the $SO(10)$ subgroup that arises at the first step of the E_6 breaking scheme of Eq. (2.1). In the conventional field assignment, the representation **16** contains the left-handed quark and lepton supermultiplets (Q and L), as well as the right-handed quarks and leptons (U , D , E and N), while the Higgs fields (H_u and H_d) and the exotic quarks Q_D and \bar{Q}_D are in the representation **10**. An alternative framework consists of having instead H_u and \bar{Q}_D lying in the **16** and L and D in the **10** representation. According to whether one chooses the standard or unconventional assignment, the phenomenology of the Z' boson may be different. In the following, we shall adopt the standard $SO(10)$ representation choices, with the exotic quarks lying in the **10** representation. Nevertheless, the unconventional scenario can be easily recovered by redefining $\theta_{E_6} \rightarrow \theta_{E_6} + \arctan \sqrt{15}$ in Eq. (2.2) [29].

The **16** representation of $SO(10)$ is then decomposed in terms of those of $SU(5)$ as $\mathbf{16} = \mathbf{10} \oplus \bar{\mathbf{5}} \oplus \mathbf{1}$. The **10** representation of $SU(5)$ is suitable to include right-handed up-type quark and charged-lepton supermultiplets, together with the weak doublets of left-handed quarks, whereas the $\bar{\mathbf{5}}$ representation contains right-handed down quarks and left-handed lepton supermultiplets; the **1** representation includes right-handed (s)neutrinos [30]. The UMSSM superpotential is thus given, all flavor indices being omitted for clarity, by:

$$W_{\text{UMSSM}} = U \mathbf{Y}_u Q H_u - D \mathbf{Y}_d Q H_d - E \mathbf{Y}_e L H_d + N \mathbf{Y}_\nu L H_u + \lambda H_u H_d S. \quad (2.3)$$

The Yukawa interactions are encoded in a set of four 3×3 matrices in flavor space, \mathbf{Y}_u , \mathbf{Y}_d , \mathbf{Y}_l and \mathbf{Y}_ν , and the strength of the supersymmetric Higgs self-interactions is described by the λ parameter. After the breaking of the $U(1)'$ symmetry, this λ -term induces the dynamical generation of an effective μ -term (noted μ_{eff} in the following) that allows for the resolution of the so-called MSSM μ -problem². As supersymmetry has to be softly broken, we introduce in the Lagrangian explicit mass terms for all gaugino and scalar fields,

$$\begin{aligned} \mathcal{L}_{\text{soft}}^{(\text{masses})} = & \frac{1}{2} \left(M_1 \lambda_{\tilde{B}} \cdot \lambda_{\tilde{B}} + M_2 \lambda_{\tilde{W}} \cdot \lambda_{\tilde{W}} + M_3 \lambda_{\tilde{g}} \cdot \lambda_{\tilde{g}} + M_4 \lambda_{\tilde{B}'} \cdot \lambda_{\tilde{B}'} + \text{h.c.} \right) - m_{H_d}^2 h_d^\dagger h_d \\ & - m_{H_u}^2 h_u^\dagger h_u - \frac{1}{2} m_s^2 s^2 - m_{\tilde{q}}^2 \tilde{q}^\dagger \tilde{q} - m_{\tilde{d}}^2 \tilde{d}^\dagger \tilde{d} - m_{\tilde{u}}^2 \tilde{u}^\dagger \tilde{u} - m_{\tilde{l}}^2 \tilde{l}^\dagger \tilde{l} - m_{\tilde{e}}^2 \tilde{e}^\dagger \tilde{e} - m_{\tilde{\nu}}^2 \tilde{\nu}^\dagger \tilde{\nu}, \end{aligned} \quad (2.4)$$

where the $U(1)_Y$, $U(1)'$, $SU(2)_L$ and $SU(3)_c$ gaugino Weyl fermions are denoted by $\lambda_{\tilde{B}}$, $\lambda_{\tilde{B}'}$, $\lambda_{\tilde{W}}$ and $\lambda_{\tilde{g}}$, respectively, and where h_d , h_u , s , \tilde{q} , \tilde{d}^\dagger , \tilde{u}^\dagger , \tilde{l} , \tilde{e}^\dagger and $\tilde{\nu}^\dagger$ are the scalar

weak isospin quantum numbers allowing for a superpotential interaction term involving ordinary quarks and inducing rapid proton decay. Their mass must thus be comparable to the GUT scale to prevent the proton from decaying too quickly [8].

² μ_{eff} is related to λ and to the vacuum expectation value of the scalar singlet s via $\mu_{\text{eff}} = \lambda \langle s \rangle$.

components of the H_d , H_u , S , Q , D , U , L , E and N superfields. The set of M_i and m_i parameters moreover denote the soft gaugino and scalar mass parameters, respectively.

Additional soft terms, related to trilinear scalar interactions, are also present and can be derived from the structure of the superpotential,

$$\mathcal{L}_{\text{soft}}^{(\text{tril.})} = -A_\lambda s h_u h_d + \tilde{d}^\dagger \mathbf{A}_d \tilde{q} h_d + \tilde{e}^\dagger \mathbf{A}_e \tilde{l} h_d - \tilde{u}^\dagger \mathbf{A}_u \tilde{q} h_u - \tilde{\nu}^\dagger \mathbf{A}_\nu \tilde{l} h_u + \text{h.c.} , \quad (2.5)$$

where the \mathbf{A}_e , \mathbf{A}_ν , \mathbf{A}_d and \mathbf{A}_u 3×3 matrices stand for the strengths of the soft Higgs-boson interactions with charged sleptons, sneutrinos and down-type squarks and up-type squarks, respectively. The A_λ parameter is finally related to the trilinear soft multi-Higgs boson coupling.

In order to calculate the sfermion masses, one would need to set up an explicit framework for supersymmetry breaking, such as a gauge-, gravity- or anomaly-mediated mechanisms, which goes beyond the goals of the present paper. We only recall that supersymmetry can be spontaneously broken if the so-called D -term and/or F -term in the scalar potential have non-zero vacuum expectation values. The F -terms are proportional to the SM particle masses, and are therefore important only for stop quarks, whereas D -terms are relevant for both light and heavy sfermions and contain contributions due to electroweak symmetry breaking and, in case of extension of the MSSM, to the Higgs bosons which break the extended symmetry [21, 24, 25]. Hereafter, we account for F - and D -term corrections to the sfermion masses, but do not present their explicit expressions, for the sake of brevity.

After the spontaneous breaking of the symmetry group down to electromagnetism, the W , Z and Z' bosons get massive and the photon stays massless. In general, for a $U(1)'$ extension of the SM, there is mixing between the Z and Z' eigenstates, parameterized by a mixing angle $\alpha_{ZZ'}$. However, electroweak precision data strongly constrain $\alpha_{ZZ'}$ to be very small [31]. At tree level, the squared masses of the Z and Z' bosons are given by:

$$\begin{aligned} M_Z^2 &= \frac{g_1^2 + g_2^2}{2} \left(\langle h_u^0 \rangle^2 + \langle h_d^0 \rangle^2 \right) \\ M_{Z'}^2 &= 2g'^2 \left(Q_S'^2 \langle s \rangle^2 + Q_{H_u}'^2 \langle h_u^0 \rangle^2 + Q_{H_d}'^2 \langle h_d^0 \rangle^2 \right) , \end{aligned} \quad (2.6)$$

where h_d^0 and h_u^0 stand for the neutral components of the down-type and up-type Higgs fields h_d and h_u and g_1 , g_2 and g' are the coupling constants of the $U(1)_Y$, $SU(2)_L$ and $U(1)'$ gauge groups, respectively. As discussed, *e.g.*, in Ref. [8], whenever the singlet s has a large vacuum expectation value (which contributes only to the Z' mass), as will be the case hereafter, $M_Z^2 \ll M_{Z'}^2$.

In the Higgs sector, after electroweak symmetry breaking, one is left with two charged H^\pm and four neutral scalar bosons, namely one pseudoscalar A and three neutral h , H and H' scalars, where the novel H' is connected to the extra $U(1)'$ symmetry and is typically much heavier than the Z' boson. With respect to the MSSM, one has two extra neutralinos, related to the supersymmetric partners of Z' and H' bosons, which yields a total of six $\tilde{\chi}_1^0, \dots, \tilde{\chi}_6^0$ neutralino states. As discussed in Ref. [25], the new $\tilde{\chi}_5^0$ and $\tilde{\chi}_6^0$ eigenstates are often too heavy to contribute to the Z' phenomenology at the LHC. As the new Z' is electrically neutral, the chargino sector stays instead unchanged with respect to the MSSM.

On top of mass mixings, both $U(1)_Y$ and $U(1)'$ bosons are allowed to mix kinetically [32]. The corresponding Lagrangian reads, in terms of the gauge boson component fields,

$$\mathcal{L}_{\text{kin}} = -\frac{1}{4}\hat{B}^{\mu\nu}\hat{B}_{\mu\nu} - \frac{1}{4}\hat{Z}'^{\mu\nu}\hat{Z}'_{\mu\nu} - \frac{\sin\chi}{2}\hat{B}^{\mu\nu}\hat{Z}'_{\mu\nu}, \quad (2.7)$$

where $\hat{B}_{\mu\nu}$ and $\hat{Z}'_{\mu\nu}$ are the $U(1)_Y$ and $U(1)'$ boson field strength tensors, respectively, and χ is the kinetic mixing angle. In order to understand the physical implications of the kinetic mixing, it is necessary to diagonalize the field strengths, which is achieved via a $GL(2, \mathbb{R})$ rotation,

$$\begin{pmatrix} \hat{B}_\mu \\ \hat{Z}'_\mu \end{pmatrix} = \begin{pmatrix} 1 & -\tan\chi \\ 0 & \frac{1}{\cos\chi} \end{pmatrix} \begin{pmatrix} B_\mu \\ Z'_\mu \end{pmatrix}, \quad (2.8)$$

where \hat{B}_μ and Z'_μ are the original $U(1)$ and $U(1)'$ gauge fields, with non-diagonal kinetic terms, while B_μ and Z'_μ have now canonical diagonal kinetic terms. As discussed in Refs. [8, 32], for $M_Z^2 \ll M_{Z'}^2$ and small values of χ , the impact of the kinetic mixing on the gauge boson masses is negligible. It nonetheless can have a significant effect on the coupling of the Z' boson with fermions. In fact, the interaction Lagrangian of the fields \hat{B}_μ and \hat{Z}'_μ with a generic fermion ψ_i , with charges Y_i and Q'_i under the $U(1)$ and $U(1)'$ groups, is given by

$$\mathcal{L}_{\text{int}} = -\bar{\psi}_i \gamma^\mu (g_1 Y_i \hat{B}_\mu + g' Q'_i \hat{Z}'_\mu) \psi_i, \quad (2.9)$$

which can then be rewritten in terms of B_μ and Z'_μ as

$$\mathcal{L}_{\text{int}} = -\bar{\psi}_i \gamma^\mu (g_1 Y_i B_\mu + g' \bar{Q}_i Z'_\mu) \psi_i, \quad (2.10)$$

where

$$\bar{Q}_i = Q'_i \sec\chi - \frac{g_1}{g'} Y_i \tan\chi. \quad (2.11)$$

Leptophobic scenarios can hence be obtained requiring $\bar{Q}_L = \bar{Q}_E = 0$ [33–35]. Since $Y_L = -1/2$ and $Y_E = 1$, Eq. (2.11) dictates that leptophobia can be achieved only if $Q'_E = -2Q'_L$: this relation between the doublet and singlet leptonic charges is typical for the $U(1)_\eta$ configuration, as shown in Table 2. Furthermore, if one assumes, as will be done in the following, the typical GUT-inspired relation between the $U(1)$ and $U(1)'$ couplings $g_1(M_{Z'})/g'(M_{Z'}) = \sqrt{3/5}$, then leptophobia requires the additional condition $\sin\chi \approx -0.3$. As a result, we expect leptophobic Z' models to naturally arise for E_6 mixing angles in the neighbourhood of

$$\theta_{E_6} \simeq \theta_\eta \pm n\pi, \quad n = 0, 1, 2, 3, \dots, \quad (2.12)$$

with the Z' -boson leptonic couplings being either exactly zero or very suppressed.

2.2 Parameter-space scan and constraints

UMSSM theories rely on numerous free parameters so that simplifying assumptions are in order for a practical parameter-space exploration. Hereafter, we impose minimal flavor violation, so that all the flavor-violating parameters of the soft supersymmetry-breaking Lagrangian are considered as vanishing, and enforce unification boundary conditions on the remaining soft parameters.

Parameter	Scanned range	Parameter	Scanned range
M_0	$[0, 3]$ TeV	μ_{eff}	$[-2, 2]$ TeV
$M_{1/2}$	$[0, 5]$ TeV	A_λ	$[-7, 7]$ TeV
A_0	$[-3, 3]$ TeV	$M_{Z'}$	$[1.98, 5.2]$ TeV
$\tan \beta$	$[0, 60]$	θ_{E_6}	$[-\pi, \pi]$

Parameter	Scanned range	Parameter	Scanned range
$m_{\tilde{q}, \tilde{u}, \tilde{d}}^2$	$[0, 16]$ TeV ²	$M_{1,2,3,4}$	$[0, 3]$ TeV
$m_{\tilde{e}, \tilde{l}}^2$	$[0, 1]$ TeV ²	$m_{\tilde{\nu}}^2$	$[-6.8, 9]$ TeV ²

Table 3. Ranges over which we allow the parameters in Eqs (2.15) and (2.17) to vary. As discussed in the text, for coupling unification at GUT scale, only the quantities in the top panel are varied.

In the first class of scenarios which we investigate, unification is assumed to occur at a very high scale $M_{\text{GUT}} \approx \mathcal{O}(10^{16})$ GeV and all parameters are then run down to $M_{Z'}$ according to renormalization group evolution. More precisely, all gauge couplings are assumed to unify at a given high scale and the $U(1)'$ coupling is enforced to satisfy

$$g'(M_{\text{GUT}}) = \sqrt{\frac{5}{3}} g_1(M_{\text{GUT}}). \quad (2.13)$$

Furthermore, all scalar masses are set to a common value M_0 , whilst all gaugino masses are taken equal to another universal mass $M_{1/2}$. All trilinear soft couplings are assumed to be proportional to the respective Yukawa coupling matrices with a universal proportionality factor A_0 , so that

$$\mathbf{A}_i = \mathbf{Y}_i A_0 \quad \text{for } i = e, \nu, d, u. \quad (2.14)$$

In the Higgs sector, we fix the values of the effective μ_{eff} parameter, the ratio of the vacuum expectation values of the neutral components of the two Higgs doublets $\tan \beta = v_u/v_d$, the trilinear soft coupling A_λ , as well as the Z' mass $M_{Z'}$. Finally, the diagonal entries of the neutrino Yukawa coupling matrices are set to a very small value, $\mathcal{O}(10^{-11})$, in such a way as to ignore the sneutrino soft trilinear interactions. The ensemble of free parameters considered in our exploration of the UMSSM parameter space is thus given by

$$\left\{ M_0, M_{1/2}, A_0, \tan \beta, \mu_{\text{eff}}, A_\lambda, M_{Z'}, \theta_{E_6} \right\}, \quad (2.15)$$

where we have additionally included the E_6 mixing angle θ_{E_6} . We vary those parameters over the ranges given in the top panel of Table 3.

In the second class of scenarios considered in this work, unification is imposed at the Z' mass scale. In this case, we just enforce the unification of the trilinear couplings as in Eq. (2.14) and set

$$g'(M_{Z'}) = \sqrt{\frac{5}{3}} g_1(M_{Z'}) , \quad (2.16)$$

Observable	Constraints	Ref.	Observable	Constraints	Ref.
M_h	$125.09 \pm 3 \text{ GeV (theo)}$	[36]	$\chi^2(\hat{\mu})$	≤ 70	-
$ \alpha_{ZZ'} $	$\mathcal{O}(10^{-3})$	[37]	$M_{\tilde{g}}$	$> 1.75 \text{ TeV}$	[38]
$M_{\tilde{\chi}_2^0}$	$> 62.4 \text{ GeV}$	[39]	$M_{\tilde{\chi}_3^0}$	$> 99.9 \text{ GeV}$	[39]
$M_{\tilde{\chi}_4^0}$	$> 116 \text{ GeV}$	[39]	$M_{\tilde{\chi}_i^\pm}$	$> 103.5 \text{ GeV}$	[39]
$M_{\tilde{\tau}}$	$> 81 \text{ GeV}$	[39]	$M_{\tilde{e}}$	$> 107 \text{ GeV}$	[39]
$M_{\tilde{\mu}}$	$> 94 \text{ GeV}$	[39]	$M_{\tilde{t}}$	$> 900 \text{ GeV}$	[40]
$\text{BR}(B_s^0 \rightarrow \mu^+ \mu^-)$	$[1.1 \times 10^{-9}, 6.4 \times 10^{-9}]$	[41]	$\frac{\text{BR}(B \rightarrow \tau \nu_\tau)}{\text{BR}_{SM}(B \rightarrow \tau \nu_\tau)}$	$[0.15, 2.41]$	[42]
$\text{BR}(B^0 \rightarrow X_s \gamma)$	$[2.99, 3.87] \times 10^{-4}$	[43]			

Table 4. Experimental constraints imposed within our scanning procedure in order to determine the parameter-space regions of interest.

all scalar and gaugino masses being kept free. The entire set of free parameters is thus here given by

$$\left\{ m_{\tilde{q}}^2, m_{\tilde{u}}^2, m_{\tilde{d}}^2, m_{\tilde{l}}^2, m_{\tilde{e}}^2, m_{\tilde{\nu}}^2, M_1, M_2, M_3, M_4, A_0, \tan \beta, \mu_{\text{eff}}, A_\lambda, M_{Z'}, \theta_{E_6} \right\}, \quad (2.17)$$

with the ranges over which those parameters vary presented in Table 3.

In our scanning procedure, we analyze all possible anomaly-free UMSSM models derived from the breaking of an E_6 gauge symmetry. We generate the particle spectrum by making use of the SARAH code, version 4.6.0 [44], and its interface to SPHENO 3.3.8 [45]. In order to test the phenomenological viability of the model, we compute various properties of the Higgs sector, such as the mass of the lightest Higgs state and the corresponding collider signal strengths by means of the HIGGSBOUNDS (version 4.3.1) and HIGGSSIGNALS (version 1.4.0) packages [46, 47]. The scan itself and the numerical analysis performed in this work have been achieved by interfacing all programs using also the PYSLHA package, version 3.1.1 [48].

The parameter space is probed by using the Metropolis–Hasting sampling method, requiring consistency with the experimental bounds on masses and decay rates shown in Table 4. In particular, we require the mass of the Standard Model Higgs boson to agree with the measurements up to an uncertainty of 3 GeV, and the χ^2 fit of the available Higgs signal strengths is bounded to be smaller than the conservative value of 70. Other constraints, connected to the bounds on the masses of supersymmetric particles and on several flavor observables, are evaluated relying on the SPHENO code. This includes in particular tests of the strict limits stemming from B -meson decays [40–42]. As for the supersymmetric sector, we enforce the LEP limits on slepton, chargino, and neutralino masses quoted in Ref. [39], while for gluinos and stops we implement the bounds set by CMS [38] and ATLAS [40], respectively.

Parameter	$U(1)'_\psi$	$U(1)'_\eta$	$U(1)'_I$	$U(1)'_N$
g'_{\min}	0.634	0.585	0.559	0.624
$\Delta g'$ [%]	0.9	7.8	6.8	1.4
$[\text{BR}(Z' \rightarrow ll)]_{\text{UMSSM}}^{\min}$ [%]	5.5	3.6	9.3	7.8
$[\text{BR}(Z' \rightarrow ll)]_{\text{USM}}^{\min}$ [%]	8.4	4.8	11.1	11.1

Table 5. g' values and dilepton branching ratios for commonly studied $U(1)'$ models with UMSSM parameters satisfying the constraints detailed in subsection 2.2. Quoted are g'_{\min} , the minimum value of $g'(M_{Z'})$, along with the corresponding spread $\Delta g'$ and the smallest possible branching ratio into leptons with (UMSSM) and without (USM) supersymmetric contributions to the Z' decays.

3 Supersymmetric Z' Phenomenology

In this section, we analyze the phenomenology of the two classes of UMSSM scenarios introduced in Section 2.2. In the subsequent Section 4, specific configurations where the Z' boson is leptophobic by virtue of the kinetic mixing of $U(1)_Y$ and $U(1)'$ are in contrast investigated.

In order to apply the LHC constraints on the properties of Z' bosons, we calculate the Z' production cross section at next-to-leading order (NLO) accuracy in QCD [49, 50]. This relies on the joint use of FEYNRULES version 2.3.27 [51] and the included NLOCT package [52], as well as FEYNARTS [53], for the automatic generation of a UFO library [54] containing both tree-level and counterterm vertices necessary at NLO. This UFO model is then used by MADGRAPH5_AMC@NLO (version 2.5.5) [55] for the numerical evaluation of the hard-scattering matrix elements, which are convoluted with the NLO set of NNPDF 2.3 parton distribution functions (PDF) [56]. Using the decay table provided by the SPHENO package and assuming the narrow-width approximation, we compare our predictions with the ATLAS limits on Z' bosons in the dilepton mode [17] in order to estimate the impact of supersymmetric decay channels.

3.1 Scenarios With High-Scale Boundary Conditions

In this subsection, we focus on our first class of UMSSM scenarios where the proportionality between g' and g_1 is imposed at the GUT scale and where all free parameters in Eq. (2.15) are fixed at M_{GUT} and then evolved down to the Z' scale by means of renormalization group equation.

We have found that some parameter regions satisfying the constraints in Table 4 exist for a wide set of values of the E_6 mixing angle θ_{E_6} . The LHC collaborations typically use the rate $\sigma B \equiv \sigma(pp \rightarrow Z') \times \text{BR}(Z' \rightarrow l^+ l^-)$ to obtain the exclusion limits on the Z' mass. For the sake of exploring possible loopholes in the Z' searches, we are therefore especially interested in scenarios which minimize the σB product, namely featuring small values of the g' coupling and of the $\text{BR}(Z' \rightarrow l^+ l^-)$ branching ratio. In Table 5, we

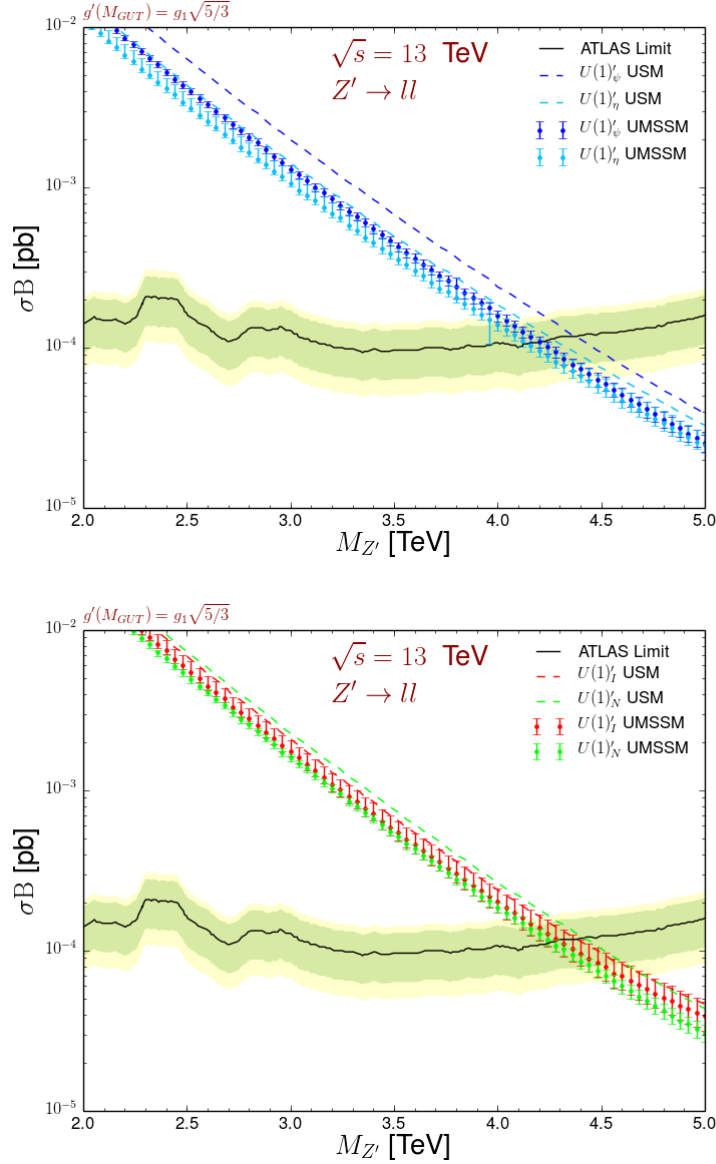


Figure 1. Comparison of our predictions for the $\sigma(pp \rightarrow Z') \times \text{BR}(Z' \rightarrow ll)$ product, in the scenario where the model boundary conditions are set at M_{GUT} , with the ATLAS dilepton yield [17] at the 1σ (green) and 2σ (yellow) levels. In the upper panel, we present the results for the $U(1)'_\psi$ and $U(1)'_\eta$ models, and in the lower panel, we focus on the $U(1)'_I$ and $U(1)'_N$ models. The dots with error bands correspond to the UMSSM case, while the dashed lines do not include supersymmetry (USM). NLO corrections to $\sigma(pp \rightarrow Z')$ are accounted for in both cases and the spread in the UMSSM results includes the effects of the parameter scan as well as the theoretical error originating from scale and PDF variations.

quote, for a few $U(1)'$ models, the minimum value of g' at the $M_{Z'}$ scale, as obtained after scanning the particle masses in the ranges presented in Table 3, imposing the constraints of Table 4 and accounting for proper threshold matching conditions in the evolution equations.

We also present the spread $\Delta g'$ around g'_{\min} and the minimum branching fraction of Z' decays into dilepton final states, including supersymmetric channels (UMSSM) and without supersymmetry (USM). In the table, we have discarded the models $U(1)'_\chi$ and $U(1)'_S$. As discussed, *e.g.*, in Refs. [24, 26], $U(1)'_\chi$ models are ill-defined in supersymmetry as they typically lead to unphysical sfermion masses after adding to the soft masses the D -term contributions. As to $U(1)'_S$, it may be theoretically acceptable, but we were not able to find scenarios capable of satisfying the constraints of Table 4. From Table 5, we learn that the deviations of g' from g'_{\min} are rather small, with $\Delta g'$ being of at most about 8%. But the impact of the inclusion of supersymmetric decays on the dilepton branching fraction is remarkable for most models. In the $U(1)'_\psi$ and $U(1)'_\eta$ scenarios, for example, $\text{BR}(Z' \rightarrow ll)$ decreases by about 35% and 25%, respectively, once decays into sfermions and gauginos are accounted for. Nevertheless, all models still exhibit substantial dilepton Z' decay rates, varying between 3% and 10%.

In Fig. 1 we compare the ATLAS limits on high-mass dileptons at the 1σ (green) and 2σ (yellow) levels with our predictions for σB , obtained in the context of $U(1)'_\psi$ and $U(1)'_\eta$ (upper panel), as well as $U(1)'_I$ and $U(1)'_N$ (lower panel) gauge groups, in the range $2 \text{ TeV} < M_{Z'} < 5 \text{ TeV}$. We consider both supersymmetric (markers with error bars) and non-supersymmetric cases (dashed line) and include NLO QCD corrections to the production cross section $\sigma(pp \rightarrow Z')$. The error bars around the supersymmetric results include two contributions: first, they account for the spread covered in the scan and second, they include the theoretical uncertainties stemming from traditional scale and parton density variations in the NLO computation. We found that the latter uncertainty varies from 5% for Z' masses of about 2 TeV and goes up to 20% for $M_{Z'} \simeq 5 \text{ TeV}$. We observe that the impact of supersymmetric decays on the excluded $M_{Z'}$ values runs from about 100 GeV (Z'_η) to 200 GeV (Z'_ψ and Z'_N), while the errors on the Z'_I dilepton rate in the UMSSM are too large to discriminate it from the non-supersymmetric case. Overall, Z' bosons lighter than 4 TeV are still strongly disfavored by ATLAS data, regardless of the $U(1)'$ model.

In Fig. 2 (upper panel), we reexpress the same results by emphasizing the dependence of σB on the dilepton branching fraction, by superimposing the predictions of the different $U(1)'$ realizations, regardless of the actual θ_{E_6} mixing angle, and displaying the values of $\text{BR}(Z' \rightarrow ll)$ by means of different colors. We find that the dilepton rate varies between 4% and 12%, and that the yielded exclusion masses are roughly between 4 and 4.5 TeV.

In the lower panel of Fig. 2, we present instead the distribution of the allowed Z' -boson masses as a function of the E_6 mixing angle, with the value of the g' coupling for each scenario indicated by a color code. In order to determine the allowed regions, we first impose the experimental constraints in Table 4 and then the exclusion limits coming from the direct comparison with the ATLAS data in Fig. 1. The points ruled out by the ATLAS results are shown in grey. We observe, similarly to the findings of Ref. [26], that only $|\theta_{E_6}|$ values in the intervals $[0, \pi/4]$ and $[3/4\pi, \pi]$ can accommodate all the imposed experimental constraints. Outside of these regions, the $U(1)'$ charge of the extra singlet supermultiplet S is in fact close to zero so that either the SM-like Higgs boson or the Z' boson, or even both, are predicted to be too light with respect to current data. In particular, Fig. 2 (lower panel) dictates that models $U(1)'_\chi$ and $U(1)'_S$ are largely ruled out by the current data

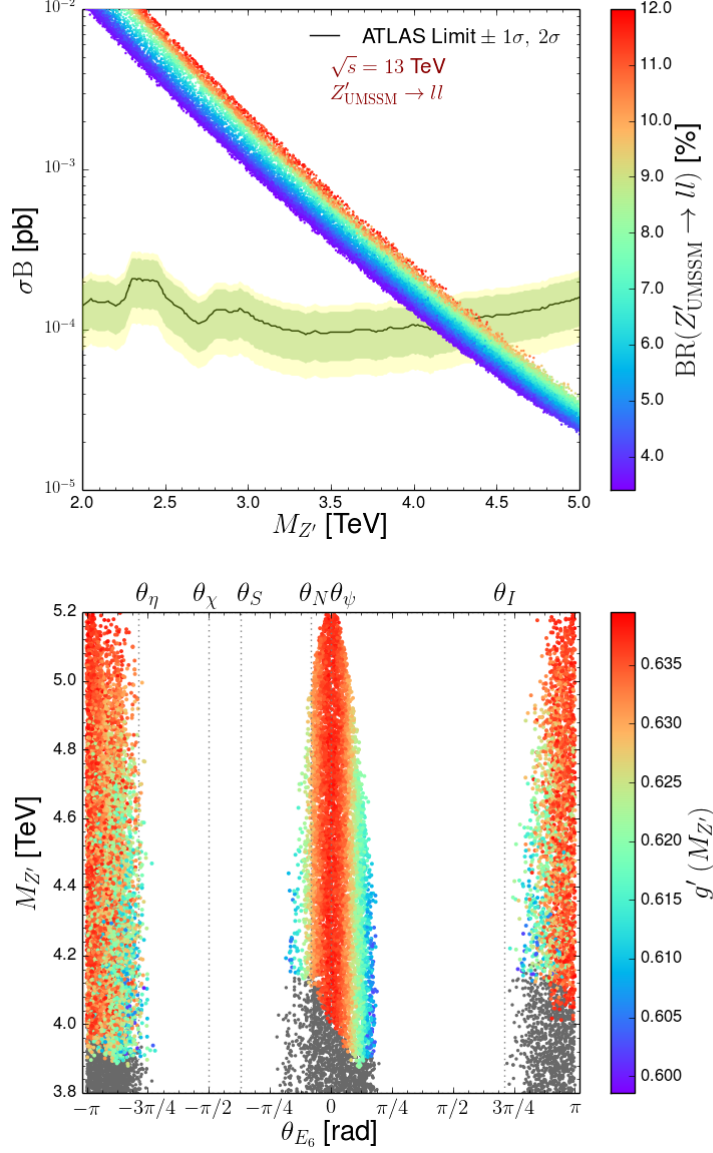


Figure 2. In the upper panel, we compare the σB rate with ATLAS data, regardless of the specific $U(1)'$ group and emphasizing the values of the $Z' \rightarrow ll$ branching ratio. In the lower panel, we show the correlations between the Z' -boson mass and the θ_{E_6} mixing angle for all points satisfying the constraints detailed in Section 2.2. Points that are excluded at the 2σ level by the recent ATLAS search for Z' in the dilepton mode [17] are shown in grey, whilst the value of the $U(1)'$ coupling strength is shown otherwise. Both figures refer to the scenario where couplings unify at M_{GUT} .

(see also the above discussion), while $U(1)'_I$ is only marginally consistent. As a whole, after adding the recent ATLAS constraints [17] (the grey points), it turns out once again that scenarios exhibiting a Z' boson lighter than 4 TeV can hardly ever be realized, the corresponding parameter-space regions getting more and more restricted.

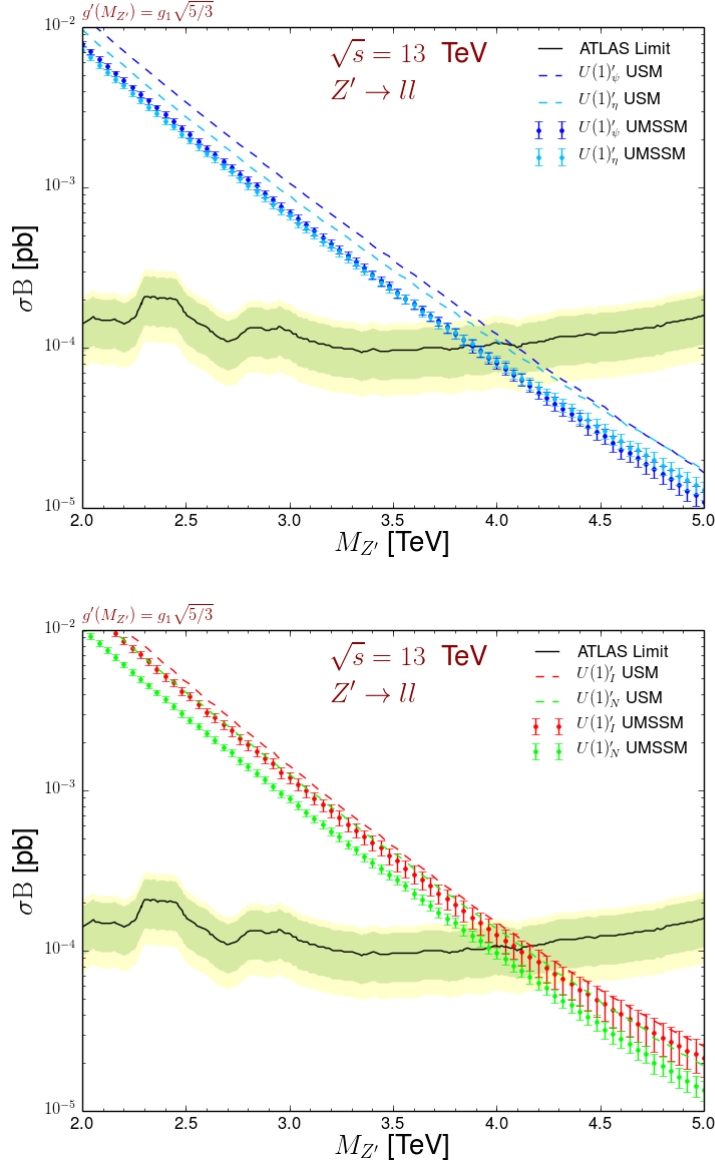


Figure 3. As in Fig. 1, but for the scenario where the condition $g' = \sqrt{5/3}g_1$ is imposed at $M_{Z'}$.

3.2 Scenarios with Low-Scale Boundary Conditions

In this subsection, we focus on the second class of scenarios, wherein the input parameters, given in Eq. (2.17), are provided at the Z' mass scale and where the $U(1)'$ coupling reads

$$g'(M_{Z'}) = \sqrt{\frac{5}{3}} g_1(M_{Z'}) \approx 0.47, \quad (3.1)$$

for all models satisfying the constraints imposed in subsection 2.2. Comparing Eq. (3.1) with the minimal values for $g'(M_{Z'})$ quoted in Table 5, we learn that, for low-scale boundary

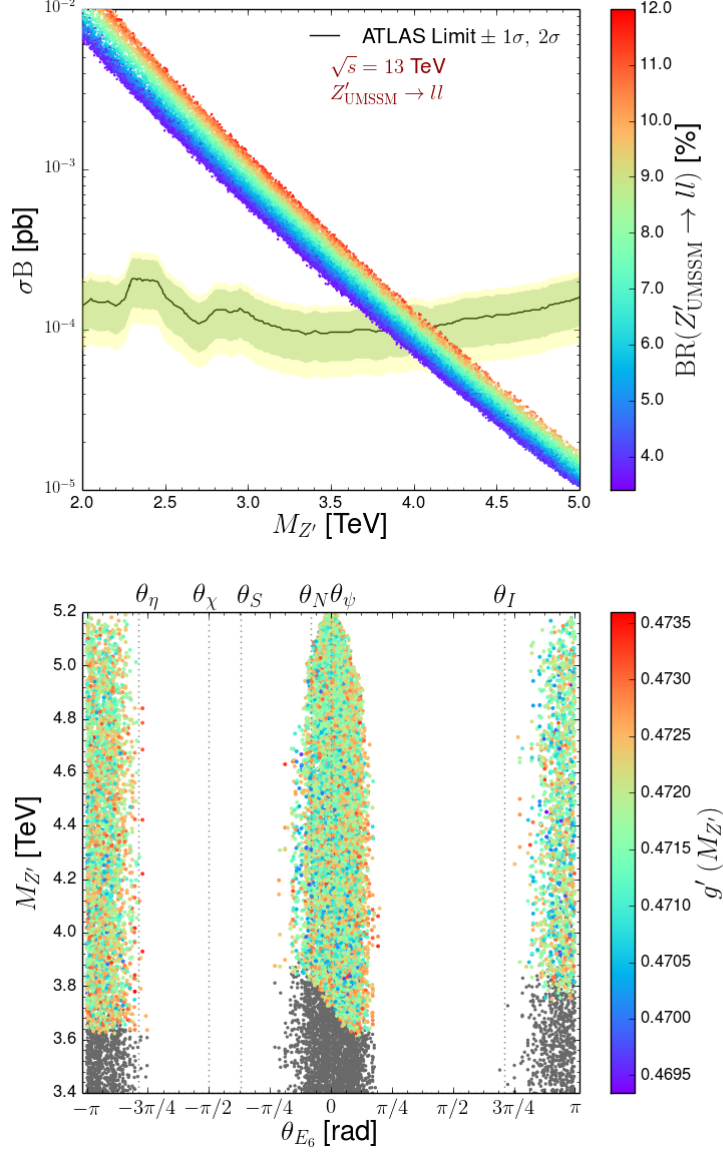


Figure 4. As in Fig. 2, but for coupling unification at $M_{Z'}$.

conditions, g' is substantially smaller. Therefore, the Z' -production cross section is lower than for scenarios where boundary conditions are provided at the GUT scale M_{GUT} .

As a consequence, the inferred Z' mass exclusion limits are reduced by about 200–300 GeV with respect to the high-scale unification case, as can be seen in Fig. 3, where the ATLAS limits are compared with the UMSSM predictions for $U(1)'_\psi$, $U(1)'_\eta$ (upper panel), and $U(1)'_N$ and $U(1)'_I$ (lower panel) models. Since the g' value is roughly the same as in the non-supersymmetric case, the overall impact of the inclusion of supersymmetric decays is similar to that found in the high-scale boundary framework, namely a reduction of the bounds on the Z' boson mass by about 200 GeV. As observed for the other class

of scenarios, the models with the highest impact of novel decay modes are the $U(1)'_\eta$ and $U(1)'_N$ ones, while the errors are too large to appreciate the effect of non-standard decays in σB for the $U(1)'_I$ case. Our analysis then confirms the finding of Ref. [27], which compared UMSSM predictions in the low-scale unification framework with 8 TeV LHC limits and obtained an effect of similar magnitude on the excluded masses.

As for the high-scale unification case, we present in Fig. 4 (upper panel) the comparison of σB with the ATLAS data, scanning through the whole parameter space and displaying in different color codes the values of $\text{BR}(Z' \rightarrow ll)$. Fig. 4 (lower panel) shows instead the correlations between the allowed $M_{Z'}$ values and θ_{E6} , accounting for both indirect constraints and direct ATLAS exclusion limits, the latter given by the grey-shaded area. The results in Fig. 4 are qualitatively similar to those presented in Fig. 2. However, as anticipated before, the g' value is smaller, so that the ATLAS constraints on $M_{Z'}$ are milder. Values of $M_{Z'} \gtrsim 3.6$ TeV are hence still allowed. Likewise, regarding specific $U(1)'$ models, $U(1)'_\chi$ and $U(1)'_S$ are ruled out, while the other setups are still permitted and worth to be further explored.

4 Leptophobic Z' Scenarios in UMSSM Models

The results presented in the previous section have shown that the inclusion of supersymmetric decays has a substantial effect on the Z' searches and exclusion limits, but nevertheless the ATLAS bounds originating from the dilepton channel strongly constrain any phenomenologically viable UMSSM realization. Furthermore, the very fact that the Z' boson has to be quite heavy impacts all sfermion masses through the $U(1)'$ D -terms, which may even lead to discarding some scenarios, such as $U(1)'_\chi$, as leading to unphysical sfermion spectra. All LHC constraints studied so far can, however, be evaded by enforcing the Z' boson to be leptophobic. In these scenarios, resonance searches in the dijet final state become the main probes of the new boson, Run II results for the top-antitop mode including the analysis of the full 2016 dataset being still not available. Dijet bounds are however much weaker, as described in Refs. [19, 20].

Before discussing the phenomenology of leptophobic Z' bosons within supersymmetry, in Fig. 5 we compare the CMS high-mass dijet yield from Ref. [20] with our predictions for $\sigma(pp \rightarrow Z') \times \text{BR}(Z' \rightarrow q\bar{q})$, obtained after scanning the UMSSM parameters as described in Table 3 and imposing the constraints of Table 4, for scenarios with high-scale (upper panel) and low-scale (lower panel) boundary conditions. As in the dilepton channel, the production cross section is calculated at NLO and the values of the dijet branching ratios are characterized by different color codes. For the sake of consistency with the experimental analysis, the σB rate is multiplied by an acceptance factor $A \simeq 0.6$ and the fraction of $Z' \rightarrow t\bar{t}$ events is not included in the calculation.

From Fig. 5, one learns that the computed σBA is always below the CMS exclusion limits in the range $2 \text{ TeV} < M_{Z'} < 5 \text{ TeV}$ at the 95% confidence level in both frameworks of coupling unification, once accounting for supersymmetric Z' decays. One can, therefore, envisage than even much lighter Z' bosons could be allowed by data when leptophobic UMSSM realizations, such as those introduced in Section 2.1, are considered.

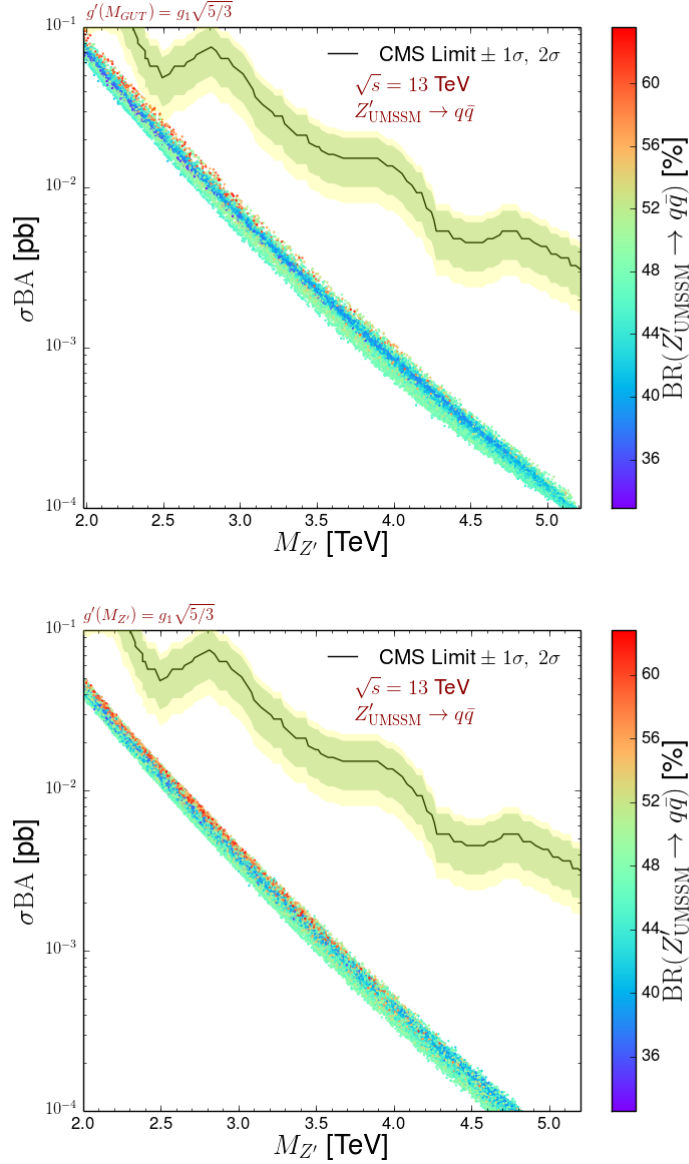


Figure 5. Z' production cross section multiplied by the dijet branching ratio and by the acceptance $A \simeq 0.6$, for the first (upper panel) and second (lower panel) class of scenarios investigated in this work. We compare NLO QCD theoretical predictions to the bounds obtained by the CMS collaboration [20] at the 1σ (green) and 2σ (yellow) level. The actual Z' dijet branching ratio is indicated with the color code.

Hereafter we focus on the second class of UMSSM scenarios, *i.e.*, coupling unification at the $M_{Z'}$ scale, and add to the list of free parameters in Eq. (2.17) the kinetic mixing angle $\sin \chi$, defined through Eq. (2.8), that we allow to vary in the $[-1, 1]$ window. In Fig. 6, we present the value of the Z' dilepton branching ratio, scanning the parameter space as presented in Section 2.2, in terms of the mixing angle θ_{E_6} and $\sin \chi$. In agreement with Eq. (2.11), we realize that values of $\sin \chi$ around ± 0.3 can lead to leptophobia whenever the

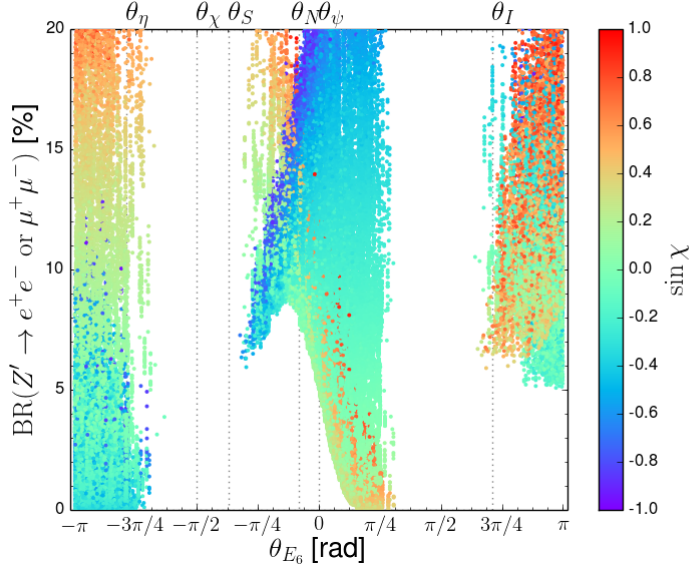


Figure 6. Correlations between the Z' -boson branching ratio into a dilepton system and the θ_{E_6} mixing angle featured by all points satisfying the constraints detailed in Section 2.2 and for UMSSM scenarios where the input parameters are fixed at the Z' mass scale (second class of considered scenarios). The value of the sine of the kinetic mixing angle ($\sin \chi$) is indicated by the color code.

E_6 mixing angle obeys the condition in Eq. (2.12) and the $U(1)'$ charges fulfill the relation $\bar{Q}_E \approx \bar{Q}_L \approx 0$. In particular, the condition $\text{BR}(Z' \rightarrow l^+ l^-) \simeq 0$ can be achieved for $-\pi \lesssim \theta_{E_6} \lesssim -3\pi/4$, which includes the $U(1)'_\eta$ model, and for $\pi/8 \lesssim \theta_{E_6} \lesssim \pi/4$, hence in the neighborhood of $U(1)'_\psi$. The other $U(1)'$ symmetries are either ruled by the experimental data or, even in the most optimistic case, can hardly lead to dilepton rates below 5%.

Of course, these leptophobic scenarios cannot be constrained by standard Z' -boson searches in dimuons or dielectrons at the LHC, and novel strategies must be designed. In the following, we propose a selection potentially allowing to observe leptophobic light Z' bosons decaying through a supersymmetric cascade. As direct decays are forbidden, dilepton final states can arise from (Z' -mediated) chargino-pair production and subsequent decays into a charged lepton and missing energy via an intermediate W -boson, possibly off-shell, namely $\tilde{\chi}_1^\pm \rightarrow (W^\pm \rightarrow l^\pm \nu_l) \tilde{\chi}_1^0$, $\tilde{\chi}_1^0$ being the lightest neutralino. However, for the points selected by our scan procedure, the off-shell contributions are typically either negligible (when the two-body decay channel is open) or not important enough to yield a sufficient number of signal events (when the $\tilde{\chi}_1^\pm \rightarrow W^\pm \tilde{\chi}_1^0$ decay is closed). We, therefore, design an analysis assuming the presence of intermediate on-shell W -bosons, targeting thus UMSSM scenarios where the mass difference between the lightest chargino $\tilde{\chi}_1^\pm$ and the lightest neutralino $\tilde{\chi}_1^0$ is at least $M_W \simeq 80$ GeV. The signal process consists of the resonant production of a chargino pair, followed by the decay of each chargino into a charged lepton and missing energy,

$$pp \rightarrow Z' \rightarrow \tilde{\chi}_1^+ \tilde{\chi}_1^- \rightarrow l^+ l^- + \cancel{E}_T. \quad (4.1)$$

Parameter	θ_{E_6}	$\tan \beta$	μ_{eff} [GeV]	$M_{Z'}$ [TeV]	M_0 [TeV]	M_1 [GeV]
BM I	-0.79π	9.11	218.9	2.5	2.6	106.5
BM II	0.2π	16.08	345.3	2.5	1.9	186.7

Parameter	M_2 [GeV]	M_3 [TeV]	M'_1 [GeV]	A_0 [TeV]	A_λ [TeV]	$\sin \chi$
BM I	230.0	3.6	198.9	2	5.9	-0.35
BM II	545.5	5.5	551.7	1.5	5.1	0.33

Table 6. UMSSM parameters for the reference points **BM I** and **BM II**.

We focus on two optimistic signal benchmarks that are currently not excluded by data and with different $U(1)'$ properties. Both scenarios exhibit a Z' boson with a mass of about 2.5 TeV and charginos and neutralinos as light as possible, in order to maximize the branching ratios in Eq. (4.1), but with a mass splitting larger than M_W , in such a way to allow the transition $\tilde{\chi}_1^\pm \rightarrow \tilde{\chi}_1^0 W^\pm$ with real W bosons. The first scenario, that we denote **BM I**, relies on a $U(1)_\eta'$ symmetry, namely $\theta_{E_6} = -0.79\pi$, since UMSSM scenarios based on this specific gauge symmetry can be made naturally leptophobic, as shown in Fig. 6. The second scenario, dubbed **BM II**, has instead a symmetry close to the $U(1)_{\psi}'$ setup, but with a larger mixing angle, *i.e.* $\theta_{E_6} = 0.2\pi$, so that a leptophobic Z' boson can still be realized (see again Fig. 6).

The UMSSM parameters for the two points are quoted in Table 6, while Tables 7 and 8 contain the predicted masses for gluinos, squarks, sleptons, Higgses and gauginos in the reference points **BM I** and **BM II**, respectively. The branching ratios of the Z' in such representative points are listed in Table 9, omitting rates which are below 1%.

Table 6 shows that **BM II** features substantially larger values of $\tan \beta$, μ_{eff} and of the gaugino masses M_1 , M_2 , M_3 and M_4 , while M_0 and the trilinear couplings A_0 and A_λ are smaller than in **BM I**. Comparing Tables 7 and 8, one learns that in **BM I** the squarks have masses between 3 and 4 TeV, while in **BM II** they are on average more than 1 TeV heavier. Charged sleptons in **BM II** are instead lighter than in **BM I**, unlike sneutrinos, whose masses vary between about 300 GeV and 1.7 TeV in **BM I** and between 660 GeV and 1.1 TeV in **BM II**. In the Higgs sector, with the exception of the SM-like h , all Higgs bosons have masses of a few TeV and are therefore too heavy to contribute to Z' phenomenology for both benchmarks. In particular, the second lightest neutral boson H is roughly degenerate with the Z' . As for gauginos, as anticipated, the two novel neutralinos $\tilde{\chi}_5^0$ and $\tilde{\chi}_6^0$ have masses about $M_{Z'}$, thus too high to be relevant for Z' decays, while charginos and MSSM-like neutralinos are sufficiently light to possibly contribute to the Z' width. Overall, the electroweakino spectrum is more compressed in the reference point **BM I**. The mass splitting between $\tilde{\chi}_1^\pm$ and $\tilde{\chi}_1^0$ is in fact slightly above M_W in **BM I**, while

$M_{\tilde{g}}$	$M_{\tilde{d}_1}$	$M_{\tilde{u}_1}$	$M_{\tilde{s}_1}$	$M_{\tilde{c}_1}$	$M_{\tilde{b}_1}$	$M_{\tilde{t}_1}$
3745.1	2988.8	2937.3	3380.3	3025.9	3380.4	3379.4
	$M_{\tilde{d}_2}$	$M_{\tilde{u}_2}$	$M_{\tilde{s}_2}$	$M_{\tilde{c}_2}$	$M_{\tilde{b}_2}$	$M_{\tilde{t}_2}$
	3525.2	3379.4	3541.2	3699.0	3541.2	3699.0
	$M_{\tilde{e}_1}$	$M_{\tilde{e}_2}$	$M_{\tilde{\mu}_1}$	$M_{\tilde{\mu}_2}$	$M_{\tilde{\tau}_1}$	$M_{\tilde{\tau}_2}$
	171.1	345.7	196.4	392.3	239.4	409.6
	$M_{\tilde{\nu}_{e,1}}$	$M_{\tilde{\nu}_{e,2}}$	$M_{\tilde{\nu}_{\mu,1}}$	$M_{\tilde{\nu}_{\mu,2}}$	$M_{\tilde{\nu}_{\tau,1}}$	$M_{\tilde{\nu}_{\tau,2}}$
	336.4	1663.1	384.1	1674.2	401.6	1683.6
M_h	M_H	$M_{H'}$	M_A	M_{H^\pm}	$M_{\tilde{\chi}_1^+}$	$M_{\tilde{\chi}_2^+}$
122.5	2507.0	3371.5	3351.5	4335.6	177.1	302.3
	$M_{\tilde{\chi}_1^0}$	$M_{\tilde{\chi}_2^0}$	$M_{\tilde{\chi}_3^0}$	$M_{\tilde{\chi}_4^0}$	$M_{\tilde{\chi}_5^0}$	$M_{\tilde{\chi}_6^0}$
	95.5	181.3	232.2	302.4	2405.1	2602.0

Table 7. Masses of gluino, squarks, sleptons, Higgs and gauginos for the UMSSM benchmark point **BM I**. $\tilde{q}_{1,2}$, $\tilde{l}_{1,2}$ and $\tilde{\nu}_{1,2}$ are mass eigenstates and differ from the gauge eigenstates $\tilde{q}_{L,R}$, $\tilde{\ell}_{L,R}$ and $\tilde{\nu}_{L,R}$ by virtue of the mass mixing contributions that are relevant especially in the stop case. All masses are in GeV.

$M_{\tilde{g}}$	$M_{\tilde{d}_1}$	$M_{\tilde{u}_1}$	$M_{\tilde{s}_1}$	$M_{\tilde{c}_1}$	$M_{\tilde{b}_1}$	$M_{\tilde{t}_1}$
5669.3	4405.5	4141.5	4927.6	4418.1	4927.7	4926.9
	$M_{\tilde{d}_2}$	$M_{\tilde{u}_2}$	$M_{\tilde{s}_2}$	$M_{\tilde{c}_2}$	$M_{\tilde{b}_2}$	$M_{\tilde{t}_2}$
	5069.8	4927.0	5146.3	5117.1	5146.3	5117.1
	$M_{\tilde{e}_1}$	$M_{\tilde{e}_2}$	$M_{\tilde{\mu}_1}$	$M_{\tilde{\mu}_2}$	$M_{\tilde{\tau}_1}$	$M_{\tilde{\tau}_2}$
	665.1	871.5	679.2	1067.9	743.9	1075.6
	$M_{\tilde{\nu}_{e,1}}$	$M_{\tilde{\nu}_{e,2}}$	$M_{\tilde{\nu}_{\mu,1}}$	$M_{\tilde{\nu}_{\mu,2}}$	$M_{\tilde{\nu}_{\tau,1}}$	$M_{\tilde{\nu}_{\tau,2}}$
	660.4	1049.6	674.3	1079.4	739.3	1106.2
M_h	M_H	$M_{H'}$	M_A	M_{H^\pm}	$M_{\tilde{\chi}_1^+}$	$M_{\tilde{\chi}_2^+}$
127.4	2498.2	5237.8	5238.0	5238.8	343.8	593.5
	$M_{\tilde{\chi}_1^0}$	$M_{\tilde{\chi}_2^0}$	$M_{\tilde{\chi}_3^0}$	$M_{\tilde{\chi}_4^0}$	$M_{\tilde{\chi}_5^0}$	$M_{\tilde{\chi}_6^0}$
	178.1	346.9	360.0	593.2	2239.1	2785.9

Table 8. Same Table 7 but for the UMSSM benchmark point **BM II**.

Decay mode	BR [%] (BM I)	BR [%] (BM II)
$Z' \rightarrow \tilde{\chi}_1^+ \tilde{\chi}_1^-$	1.7	6.3
$Z' \rightarrow \tilde{\chi}_2^+ \tilde{\chi}_2^-$	2.1	-
$Z' \rightarrow \tilde{\chi}_1^\pm \tilde{\chi}_2^\mp$	3.9	-
$Z' \rightarrow \tilde{\chi}_2^0 \tilde{\chi}_2^0$	-	1.5
$Z' \rightarrow \tilde{\chi}_2^0 \tilde{\chi}_3^0$	1.7	3.3
$Z' \rightarrow \tilde{\chi}_3^0 \tilde{\chi}_3^0$	1.9	1.9
$Z' \rightarrow \tilde{\chi}_3^0 \tilde{\chi}_4^0$	2.2	-
$Z' \rightarrow \sum_i \tilde{\nu}_i \tilde{\nu}_i^\dagger$	-	1.6
$Z' \rightarrow hZ$	1.9	1.9
$Z' \rightarrow W^+ W^-$	3.6	3.8
$Z' \rightarrow \sum_i d_i \bar{d}_i$	15.8	14.8
$Z' \rightarrow \sum_i u_i \bar{u}_i$	39.8	40.0
$Z' \rightarrow \sum_i \nu_i \bar{\nu}_i$	23.4	22.8

Table 9. Z' decay rates for the benchmark points **BM I** (second column) and **BM II** (third column). Branching ratios below 1% are omitted.

being larger than M_W , *i.e.* about 165 GeV, in the **BM II** framework. In both cases, the decay $\tilde{\chi}_1^\pm \rightarrow W^\pm \tilde{\chi}_1^0$ can occur through on-shell W -bosons and has a branching fraction of almost 100%.

Concerning the Z' branching ratios, Table 9 shows that the branching fraction of the Z' boson decay into a $\tilde{\chi}_1^+ \tilde{\chi}_1^-$ pair, entering in the process of Eq. (4.1), is of about 2% for the scenario **BM I** and 6% for the scenario **BM II**. **BM I** allows for substantial branching fractions into other combinations of chargino pairs, while both scenarios exhibit non-negligible rates into neutralino pairs, and the **BM II** scenario also includes decays into sneutrino pairs as well. The decay rates in pairs of the lightest neutralinos, possible candidates for dark matter, are instead suppressed in both reference points. As a whole, supersymmetric decays are responsible for 12% and 15% of the Z' width in the representative points **BM I** and **BM II**, respectively.

Once our representative configurations are set, we carry out a full Monte Carlo event simulation at the LHC, for a center-of-mass energy $\sqrt{s} = 14$ TeV. Hard-scattering signal events are generated with MADGRAPH5_AMC@NLO, the matrix elements being convoluted with the NLO set of NNPDF 2.3 parton densities. The production cross section is then $\sigma(pp \rightarrow Z') \simeq 120$ fb for both benchmarks. Parton showers and hadronization are simulated by means of the PYTHIA 8 program [57] (version 8.2.19), and the response

of a typical LHC detector is modelled with the DELPHES 3 package [58] (version 3.3.2), employing the SNOWMASS parameterization [59, 60]. The resulting detector-level jets are reconstructed following the anti- k_T algorithm [61] with a radius parameter $R = 0.6$, as implemented in the FASTJET program (version 3.1.3) [62]. Moreover, we consider an average number of pile-up events of 140 and normalize our results to an integrated luminosity of 3000 fb^{-1} .

Regarding the backgrounds, we consider all processes leading to final states with two charged leptons and missing energy, such as vector-boson pairs VV , with V being a W -boson or a Z boson decaying leptonically. However, for the purpose of mimicking an actual experimental analysis, we account for processes yielding also jets which do not pass the acceptance cuts. Moreover, since our event simulation includes hadronization effects, we explore the possibility that background leptons originate from hadron decays as well. Overall, our backgrounds consist of single vector bosons (V) or vector-boson pairs (VV), possibly accompanied by jets, as well as $t\bar{t}$ and single-top events. In principle, even direct chargino production ($pp \rightarrow \chi_1^+ \chi_1^- \rightarrow l^+ l^- + \cancel{E}_T$) should be considered as a background to the supersymmetric Z' decays. Nevertheless, as pointed out in Ref. [25], the leptons produced in processes with direct charginos, unlike those coming from Z' events, are typically pretty soft or collinear to the beams. It is therefore quite easy to suppress the $pp \rightarrow \tilde{\chi}_1^+ \tilde{\chi}_1^-$ background by setting suitable cuts on the lepton transverse momenta.

Lepton and jet candidates that are considered throughout our analysis must have transverse momenta p_T^l and p_T^j and pseudorapidities η^l and η^j satisfying

$$\begin{aligned} p_T^l &\geq 20 \text{ GeV} & \text{and} & & |\eta^l| < 1.5 , \\ p_T^j &\geq 40 \text{ GeV} & \text{and} & & |\eta^j| < 2.4 . \end{aligned} \tag{4.2}$$

Moreover, in our selection strategy, we reject lepton candidates that are not at an invariant angular distance, in the transverse plane, of at least 0.4 from a jet,

$$\Delta R(j, l) > 0.4 , \tag{4.3}$$

and only focus on muons that are cleaner objects than electrons, in particular for the pseudorapidity region considered in Eq. (4.2). We finally enforce the considered muons to be isolated, so that the activity in a cone of radius $R = 0.4$ centered on each muon contains at most 15% of the muon p_T ,

$$I_{\text{rel}}^\mu < 0.15 . \tag{4.4}$$

We select events featuring two well-separated muons, since the two signal leptons l_1 and l_2 are expected to originate from two different supersymmetric cascade decays, by requiring

$$N^l = 2 \quad \text{and} \quad \Delta R(l_1, l_2) > 2.5 \tag{4.5}$$

and we veto the presence of jets, *i.e.*

$$N^j = 0 . \tag{4.6}$$

Step	Requirements	Background	BM I	BM II
0	Initial	1.7×10^{11}	8.8×10^3	1.9×10^4
1	$N^l = 2$	6.1×10^8	401	860
2	Electron veto	2.9×10^8	100	230
3	$ \eta^l < 1.5$	1.7×10^8	76	170
4	$I_{\text{rel}}^\mu < 0.15$	7.9×10^5	63	130
5	$\Delta R(l_1, l_2) > 2.5$	7.9×10^5	62	130
6	Jet veto	7.7×10^4	57	120
7	$p_T(l_1) > 300 \text{ GeV}$	44	36	71
8	$p_T(l_2) > 200 \text{ GeV}$	20	19	32
9	$\cancel{E}_T > 100 \text{ GeV}$	10	14	27
s			3.77σ	7.14σ
Z_A			3.03σ	5.05σ

Table 10. Selection strategy aiming at observing a leptophobic UMSSM Z' boson decaying into a supersymmetric cascade. For each cut, we provide the expected number of surviving events for 3000 fb $^{-1}$ of pp collisions at $\sqrt{s} = 14$ TeV for both background and signal benchmark scenarios **BM I** and **BM II**. We also quote the corresponding significances s and Z_A , as defined in Eq. (4.9), with 20% uncertainty.

Furthermore, the two signal leptons are expected to be produced from the decay of a heavy Z' with a mass well above the TeV scale. We consequently impose the transverse momenta of the two leptons to fulfill

$$p_T(l_1) > 300 \text{ GeV} \quad \text{and} \quad p_T(l_2) > 200 \text{ GeV}, \quad (4.7)$$

which are very efficient cuts to reduce the remaining SM background. We finally improve the sensitivity by requiring a large amount of missing energy,

$$\cancel{E}_T > 100 \text{ GeV}, \quad (4.8)$$

as could be expected for a signal topology where several neutrinos and neutralinos escape the detector invisibly.

The corresponding cutflows are shown in Table 10, which illustrates that, for the two benchmark scenarios under consideration, background rejection is sufficiently important for observing the signal despite the low selection efficiencies. For other possible benchmark choices (not considered in this work) featuring a heavier Z' , the smaller production total rate is expected to be compensated by a larger efficiency of the two selection cuts restricting the transverse momenta of the two selected leptons.

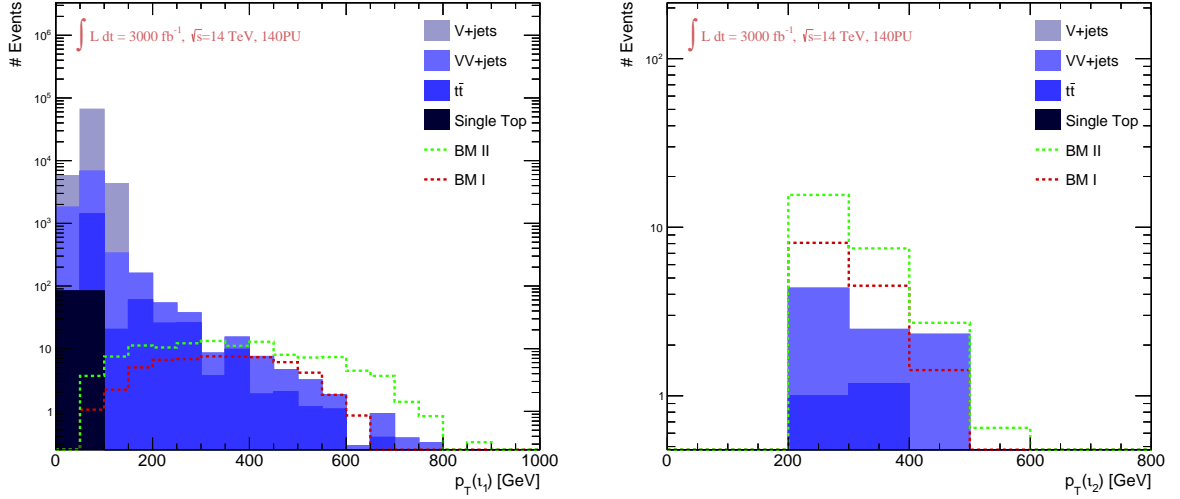


Figure 7. Transverse momentum distribution of the leading muon l_1 after applying the first 6 cuts of Table 10 (left) and of the next-to-leading muon l_2 after applying all cuts (right) for both signal scenarios and the backgrounds.

Denoting the number of selected signal and background events by S and $B \pm \sigma_B$, we make use of two standard criteria, labelled as s and Z_A , to define the LHC sensitivity to the leptophobic Z' -boson signal,

$$s = \frac{S}{\sqrt{B + \sigma_B^2}}, \quad (4.9)$$

$$Z_A = \sqrt{2 \left((S + B) \ln \left[\frac{(S + B)(S + \sigma_B^2)}{B^2 + (S + B)\sigma_B^2} \right] - \frac{B^2}{\sigma_B^2} \ln \left[1 + \frac{\sigma_B^2 S}{B(B + \sigma_B^2)} \right] \right)}.$$

While the first option (s) is rather standard, the second method (Z_A) is known to be more suitable (and conservative) when the number of background events is small [63]. The conclusions are however very similar in both cases, as can be seen from Table 10. For both significance definitions, we indeed find that the more compressed scenario **BM I** could lead to hints visible at the 3σ level, whilst the second scenario **BM II** is in principle observable at even more than 5σ . The largest LHC sensitivity to the latter scenario has a twofold origin. First, the Z' -induced chargino-pair production cross section is larger by virtue of a greater $\text{BR}(Z' \rightarrow \tilde{\chi}_1^+ \chi_1^-)$ branching ratio. Second, the heavier chargino mass typically induces harder leptons, the corresponding selection cuts being thus more efficient.

In the left panel of Fig. 7, we present the distribution in the transverse momentum of the leading muon l_1 after applying the first six cuts of Table 10. In the right panel of the figure, we in contrast show the transverse-momentum spectrum of the next-to-leading muon l_2 as resulting from the entire selection strategy. As for the $p_T(l_1)$ spectrum, all four considered backgrounds contribute at small p_T , while above 100 GeV the only surviving SM events originate from the production of VV and $t\bar{t}$ pairs. The signal spectra are rather broad and lie below the backgrounds at low $p_T(l_1)$, whereas, for $p_T(l_1) > 300$ GeV, both

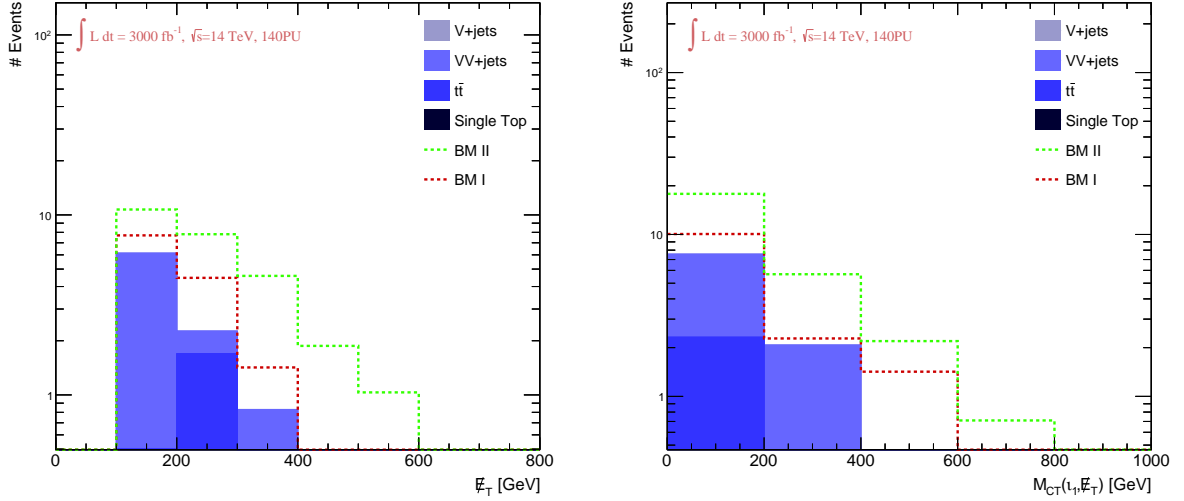


Figure 8. Left: missing transverse energy spectrum for the different components of the background and the two signal benchmarks. Right: cotransverse mass distributions for muon l_1 and invisible particles leading to missing energy (neutralinos and neutrinos). All histograms are obtained after applying all the acceptance cuts discussed in the paper.

signals **BM I** and **BM II** start to be competitive with the background, yielding comparable numbers of events. For even larger transverse momenta, say $p_T(l_1) > 500$ GeV, muons coming from supersymmetric decays of a leptophobic Z' become dominant, especially in the reference point **BM II**. After all cuts are applied, the $p_T(l_2)$ distribution is explored (Fig. 7, right). All backgrounds are further suppressed and those due to single vector-boson and single-top production are negligible. The transverse momentum spectrum is thus substantial in the $200 \text{ GeV} < p_T(l_2) < 600 \text{ GeV}$ range, with the **BM II** signal yielding the highest number of events through all p_T range and **BM I** being also quite remarkable, especially for $200 \text{ GeV} < p_T < 400 \text{ GeV}$. Overall, Fig. 7 (right) shows that the cuts which we have applied are rather efficient to discriminate the leptons in leptophobic Z' events from the Standard Model ones.

In Fig. 8 (left) we show the missing transverse energy, due to the lightest neutralinos $\tilde{\chi}_1^0$ in our signal and to neutrinos in the backgrounds, after all cuts are imposed. The \cancel{E}_T spectra of our UMSSM benchmark scenarios are well above the backgrounds, once again limited to VV and $t\bar{t}$ pairs, through the whole \cancel{E}_T range. The **BM II** configuration, in particular, is capable of yielding a few events up to $\cancel{E}_T \simeq 600$ GeV, while, above 400 GeV, the backgrounds are basically all suppressed.

We have verified that any other transverse observable, such as the M_{T2} or M_{CT} variables defined in Refs. [64–66], are not useful for improving the considered selection strategy due to the too small mass difference between the lightest chargino and the lightest neutralino. The main features of the signal topology are in this case already captured by the requirements on the lepton transverse momenta and on the missing transverse energy.

This is illustrated in Fig. 8 (right), where we present the cotransverse mass M_{CT}

distribution³ for the leading muon l_1 and all particles contributing to the missing energy (lightest neutralinos and neutrinos). The M_{CT} spectrum is qualitatively comparable to the \cancel{E}_T one. Both signals and backgrounds (VV and $t\bar{t}$) peak at similar values, although the number of events generated by Z' decays is always larger than for SM processes, and for $M_{CT} > 400$ GeV only signal events survive. Designing an analysis with a possible extra cut on M_{CT} would lead to a reduction in the significance, as both S and B would be affected in the same way. Such a new selection may, however, increase the sensitivity for spectra featuring larger mass gaps. In this work, we nevertheless choose to focus on the lighter UMSSM particle spectra that are still not excluded so far and thus more relevant for the near future.

5 Summary and Conclusions

Motivated by the latest ATLAS and CMS measurements which imposed improved lower bounds on the Z' mass, we analyzed models with an additional $U(1)'$ gauge symmetry group arising from the breaking of E_6 SUSY GUT symmetry. We explored possible loopholes in the searches carried out at the LHC. In particular, we allowed the Z' to decay into supersymmetric final states, such as gaugino pairs, and investigated scenarios where the Z' is leptophobic. In fact, as the Z' mass bounds are mostly determined by its decay into lepton pairs, the constraints would be relaxed in models in which direct leptonic decays are suppressed or even forbidden. We found that leptophobia can be achieved by accounting for the kinetic mixing between the two $U(1)$ symmetries, parameterized by an angle χ , and that, among possible $U(1)'$ groups, the model $U(1)'_\eta$, while obeying all low energy conditions on the parameter space, is most favored to be leptophobic. Our analysis was then undertaken under two possible assumptions for scale unification, the gauge couplings being imposed to unify either at the GUT scale or at $M_{Z'}$. We investigated the mass bounds and decay patterns in both cases, as well as the prospects for seeing a Z' signal above the background at the LHC, accounting for supersymmetry and leptophobia.

Concerning supersymmetry, for both high- and low-scale unification, the rates of dilepton production are smaller once we include new decay modes, which translates into a reduction of the mass exclusion limits by about 200 GeV. As for dijets, we found an even larger impact of the inclusion of supersymmetric channels, so that the LHC constraints can be evaded. Within leptophobic scenarios, observing supersymmetric Z' decays into charged leptons and missing energy would be most promising through a cascade from a primary decay into chargino pairs. We analyzed final-state signals from these intermediate states and suppressed the background by imposing a jet veto, in addition to requirements on the final-state leptons and missing energy. We chose two benchmark points in the parameter space, corresponding to different UMSSM realizations, and found that they both yield visible signals at the LHC, with a significance which varies from 3σ up to even 7σ , according to the criterion employed to estimate the LHC sensitivity.

³Given two particles of transverse energies $E_{T,1}$ and $E_{T,2}$ and transverse momenta $\vec{p}_{T,1}$ and $\vec{p}_{T,2}$, the cotransverse mass is defined as $M_{CT}^2 = (E_{T,1} + E_{T,2})^2 - (\vec{p}_{T,1} + \vec{p}_{T,2})^2$ [66].

Therefore, supersymmetric and possibly leptophobic Z' decays are capable of giving detectable dilepton signals, which can be easily discriminated from the backgrounds and from non-supersymmetric Z' events, so far employed to set the exclusion limits. Moreover, from the viewpoint of supersymmetry, Z' bosons would be a promising source of new particles, such as the charginos and neutralinos investigated in this paper, which, unlike direct production in pp collisions, would feature additional kinematic constraints set by the high Z' mass.

In summary, we believe that our study, accounting for Grand Unification Theories, supersymmetry and leptophobia altogether, should represent a useful guiding reference to explore a more general gauge structure than the Standard Model and address its incompleteness from perspectives that have not received so far proper consideration from the experimental collaborations. We demonstrated that investigating such scenarios is instead both worthwhile and feasible, as they are potentially capable of giving remarkable signals, especially in the high-luminosity phase of the LHC.

Acknowledgments

JYA thanks Altan Çakır regarding the usage of the Snowmass background samples, Florian Staub for the implementation of the model in SARAH and Özgür Şahin for providing help with the THEPLOTING software. MF acknowledges the NSERC for partial financial support under grant number SAP105354. The work of BF is partly supported by French state funds managed by the Agence Nationale de la Recherche (ANR), in the context of the LABEX ILP (ANR-11-IDEX-0004-02, ANR-10-LABX-63).

References

- [1] J. E. Kim and H. P. Nilles, *The μ Problem and the Strong CP Problem*, *Phys. Lett.* **138B** (1984) 150–154.
- [2] D. Suematsu and Y. Yamagishi, *Radiative symmetry breaking in a supersymmetric model with an extra $U(1)$* , *Int. J. Mod. Phys.* **A10** (1995) 4521–4536, [[hep-ph/9411239](#)].
- [3] M. Cvetič and P. Langacker, *New gauge bosons from string models*, *Mod. Phys. Lett.* **A11** (1996) 1247–1262, [[hep-ph/9602424](#)].
- [4] V. Jain and R. Shrock, *$U(1)$ - A models of fermion masses without a μ problem*, [[hep-ph/9507238](#)].
- [5] D. A. Demir, *Two Higgs doublet models from TeV scale supersymmetric extra $U(1)$ models*, *Phys. Rev.* **D59** (1999) 015002, [[hep-ph/9809358](#)].
- [6] M. Cvetič, D. A. Demir, J. R. Espinosa, L. L. Everett and P. Langacker, *Electroweak breaking and the μ problem in supergravity models with an additional $U(1)$* , *Phys. Rev.* **D56** (1997) 2861, [[hep-ph/9703317](#)].
- [7] D. A. Demir, G. L. Kane and T. T. Wang, *The Minimal $U(1)'$ extension of the MSSM*, *Phys. Rev.* **D72** (2005) 015012, [[hep-ph/0503290](#)].
- [8] P. Langacker, *The Physics of Heavy Z' Gauge Bosons*, *Rev. Mod. Phys.* **81** (2009) 1199–1228, [[0801.1345](#)].

- [9] F. Deppisch, A. Freitas, W. Porod and P. M. Zerwas, *Determining Heavy Mass Parameters in Supersymmetric $SO(10)$ Models*, *Phys. Rev.* **D77** (2008) 075009, [[0712.0361](#)].
- [10] J. R. Ellis, K. Enqvist, D. V. Nanopoulos, K. A. Olive, M. Quiros and F. Zwirner, *Problems for $(2,0)$ Compactifications*, *Phys. Lett.* **B176** (1986) 403–408.
- [11] U. Ellwanger, C. Hugonie and A. M. Teixeira, *The Next-to-Minimal Supersymmetric Standard Model*, *Phys. Rept.* **496** (2010) 1–77, [[0910.1785](#)].
- [12] F. del Aguila, J. de Blas and M. Perez-Victoria, *Electroweak Limits on General New Vector Bosons*, *JHEP* **09** (2010) 033, [[1005.3998](#)].
- [13] E. Salvioni, G. Villadoro and F. Zwirner, *Minimal Z' models: Present bounds and early LHC reach*, *JHEP* **11** (2009) 068, [[0909.1320](#)].
- [14] A. Leike, *The Phenomenology of extra neutral gauge bosons*, *Phys. Rept.* **317** (1999) 143–250, [[hep-ph/9805494](#)].
- [15] M. Cvetič and S. Godfrey, *Discovery and identification of extra gauge bosons*, [[hep-ph/9504216](#)].
- [16] F. del Aguila, M. Cvetič and P. Langacker, *Determination of Z' gauge couplings to quarks and leptons at future hadron colliders*, *Phys. Rev.* **D48** (1993) R969–R973, [[hep-ph/9303299](#)].
- [17] ATLAS collaboration, M. Aaboud et al., *Search for new high-mass phenomena in the dilepton final state using 36.1 fb^{-1} of proton-proton collision data at $\sqrt{s} = 13 \text{ TeV}$ with the ATLAS detector*, [[1707.02424](#)].
- [18] CMS collaboration, C. Collaboration, *Search for a high-mass resonance decaying into a dilepton final state in 13 fb^{-1} of pp collisions at $\sqrt{s} = 13 \text{ TeV}$* , .
- [19] ATLAS collaboration, M. Aaboud et al., *Search for new phenomena in dijet events using 37 fb^{-1} of pp collision data collected at $\sqrt{s} = 13 \text{ TeV}$ with the ATLAS detector*, *Phys. Rev.* **D96** (2017) 052004, [[1703.09127](#)].
- [20] CMS collaboration, A. M. Sirunyan et al., *Search for dijet resonances in proton-proton collisions at $\sqrt{s} = 13 \text{ TeV}$ and constraints on dark matter and other models*, *Phys. Lett.* **B769** (2017) 520–542, [[1611.03568](#)].
- [21] T. Gherghetta, T. A. Kaeding and G. L. Kane, *Supersymmetric contributions to the decay of an extra Z boson*, *Phys. Rev.* **D57** (1998) 3178–3181, [[hep-ph/9701343](#)].
- [22] M. Baumgart, T. Hartman, C. Kilic and L.-T. Wang, *Discovery and measurement of sleptons, binos, and winos with a Z'* , *JHEP* **11** (2007) 084, [[hep-ph/0608172](#)].
- [23] C.-F. Chang, K. Cheung and T.-C. Yuan, *Supersymmetric Decays of the Z' Boson*, *JHEP* **09** (2011) 058, [[1107.1133](#)].
- [24] G. Corcella and S. Gentile, *Heavy Neutral Gauge Bosons at the LHC in an Extended MSSM*, *Nucl. Phys.* **B866** (2013) 293–336, [[1205.5780](#)].
- [25] G. Corcella, *Phenomenology of supersymmetric Z' decays at the Large Hadron Collider*, *Eur. Phys. J.* **C75** (2015) 264, [[1412.6831](#)].
- [26] J. Y. Araz, M. Frank and B. Fuks, *Differentiating $U(1)'$ supersymmetric models with right sneutrino and neutralino dark matter*, *Phys. Rev.* **D96** (2017) 015017, [[1705.01063](#)].
- [27] G. Corcella, *Searching for supersymmetry in Z' decays*, *EPJ Web Conf.* **60** (2013) 18011, [[1307.1040](#)].

- [28] F. del Aguila, M. Quiros and F. Zwirner, *On the Mass and the Signature of a New Z*, *Nucl. Phys.* **B284** (1987) 530–556.
- [29] E. Nardi and T. G. Rizzo, *Identifying unconventional $E(6)$ models at e^+e^- colliders*, *Phys. Rev.* **D50** (1994) 203–209, [[hep-ph/9401260](#)].
- [30] R. Slansky, *Group Theory for Unified Model Building*, *Phys. Rept.* **79** (1981) 1–128.
- [31] J. Erler, P. Langacker and T.-j. Li, *The Z - Z' mass hierarchy in a supersymmetric model with a secluded $U(1)'$ breaking sector*, *Phys. Rev.* **D66** (2002) 015002, [[hep-ph/0205001](#)].
- [32] K. S. Babu, C. F. Kolda and J. March-Russell, *Implications of generalized $Z - Z'$ mixing*, *Phys. Rev.* **D57** (1998) 6788–6792, [[hep-ph/9710441](#)].
- [33] K. S. Babu, C. F. Kolda and J. March-Russell, *Leptophobic $U(1)'$ s and the $R(b) - R(c)$ crisis*, *Phys. Rev.* **D54** (1996) 4635–4647, [[hep-ph/9603212](#)].
- [34] D. Suematsu, *Vacuum structure of the μ problem solvable extra $U(1)$ models*, *Phys. Rev.* **D59** (1999) 055017, [[hep-ph/9808409](#)].
- [35] C.-W. Chiang, T. Nomura and K. Yagyu, *Phenomenology of E_6 -Inspired Leptophobic Z' Boson at the LHC*, *JHEP* **05** (2014) 106, [[1402.5579](#)].
- [36] CMS collaboration, S. Chatrchyan et al., *Observation of a new boson at a mass of 125 GeV with the CMS experiment at the LHC*, *Phys. Lett.* **B716** (2012) 30–61, [[1207.7235](#)].
- [37] J. Erler, P. Langacker, S. Munir and E. Rojas, *Improved Constraints on Z' Bosons from Electroweak Precision Data*, *JHEP* **08** (2009) 017, [[0906.2435](#)].
- [38] CMS collaboration, V. Khachatryan et al., *Search for new physics with the M_{T2} variable in all-jets final states produced in pp collisions at $\sqrt{s} = 13$ TeV*, *JHEP* **10** (2016) 006, [[1603.04053](#)].
- [39] PARTICLE DATA GROUP collaboration, K. A. Olive et al., *Review of Particle Physics*, *Chin. Phys.* **C38** (2014) 090001.
- [40] ATLAS collaboration, M. Aaboud et al., *Search for top squarks in final states with one isolated lepton, jets, and missing transverse momentum in $\sqrt{s} = 13$ TeV pp collisions with the ATLAS detector*, *Phys. Rev.* **D94** (2016) 052009, [[1606.03903](#)].
- [41] LHCb collaboration, R. Aaij et al., *First Evidence for the Decay $B_s^0 \rightarrow \mu^+ \mu^-$* , *Phys. Rev. Lett.* **110** (2013) 021801, [[1211.2674](#)].
- [42] HEAVY FLAVOR AVERAGING GROUP collaboration, D. Asner et al., *Averages of b -hadron, c -hadron, and τ -lepton properties*, [1010.1589](#).
- [43] Y. Amhis et al., *Averages of b -hadron, c -hadron, and τ -lepton properties as of summer 2016*, [1612.07233](#).
- [44] F. Staub, *SARAH 4 : A tool for (not only SUSY) model builders*, *Comput. Phys. Commun.* **185** (2014) 1773–1790, [[1309.7223](#)].
- [45] W. Porod and F. Staub, *SPheno 3.1: Extensions including flavour, CP-phases and models beyond the MSSM*, *Comput. Phys. Commun.* **183** (2012) 2458–2469, [[1104.1573](#)].
- [46] P. Bechtle, O. Brein, S. Heinemeyer, G. Weiglein and K. E. Williams, *HiggsBounds: Confronting Arbitrary Higgs Sectors with Exclusion Bounds from LEP and the Tevatron*, *Comput. Phys. Commun.* **181** (2010) 138–167, [[0811.4169](#)].

- [47] P. Bechtle, S. Heinemeyer, O. Stål, T. Stefaniak and G. Weiglein, *HiggsSignals: Confronting arbitrary Higgs sectors with measurements at the Tevatron and the LHC*, *Eur. Phys. J. C* **74** (2014) 2711, [[1305.1933](#)].
- [48] A. Buckley, *PySLHA: a Pythonic interface to SUSY Les Houches Accord data*, *Eur. Phys. J. C* **75** (2015) 467, [[1305.4194](#)].
- [49] B. Fuks, M. Klasen, F. Ledroit, Q. Li and J. Morel, *Precision predictions for Z' - production at the CERN LHC: QCD matrix elements, parton showers, and joint resummation*, *Nucl. Phys. B* **797** (2008) 322–339, [[0711.0749](#)].
- [50] B. Fuks and R. Ruiz, *A comprehensive framework for studying W' and Z' bosons at hadron colliders with automated jet veto resummation*, *JHEP* **05** (2017) 032, [[1701.05263](#)].
- [51] A. Alloul, N. D. Christensen, C. Degrande, C. Duhr and B. Fuks, *FeynRules 2.0 - A complete toolbox for tree-level phenomenology*, *Comput. Phys. Commun.* **185** (2014) 2250–2300, [[1310.1921](#)].
- [52] C. Degrande, *Automatic evaluation of UV and R2 terms for beyond the Standard Model Lagrangians: a proof-of-principle*, *Comput. Phys. Commun.* **197** (2015) 239–262, [[1406.3030](#)].
- [53] T. Hahn, *Generating Feynman diagrams and amplitudes with FeynArts 3*, *Comput. Phys. Commun.* **140** (2001) 418–431, [[hep-ph/0012260](#)].
- [54] C. Degrande, C. Duhr, B. Fuks, D. Grellscheid, O. Mattelaer and T. Reiter, *UFO - The Universal FeynRules Output*, *Comput. Phys. Commun.* **183** (2012) 1201–1214, [[1108.2040](#)].
- [55] J. Alwall, R. Frederix, S. Frixione, V. Hirschi, F. Maltoni, O. Mattelaer et al., *The automated computation of tree-level and next-to-leading order differential cross sections, and their matching to parton shower simulations*, *JHEP* **07** (2014) 079, [[1405.0301](#)].
- [56] R. D. Ball et al., *Parton distributions with LHC data*, *Nucl. Phys. B* **867** (2013) 244–289, [[1207.1303](#)].
- [57] T. Sjöstrand, S. Ask, J. R. Christiansen, R. Corke, N. Desai, P. Ilten et al., *An Introduction to PYTHIA 8.2*, *Comput. Phys. Commun.* **191** (2015) 159–177, [[1410.3012](#)].
- [58] DELPHES 3 collaboration, J. de Favereau, C. Delaere, P. Demin, A. Giammanco, V. Lemaître, A. Mertens et al., *DELPHES 3, A modular framework for fast simulation of a generic collider experiment*, *JHEP* **02** (2014) 057, [[1307.6346](#)].
- [59] J. Anderson et al., *Snowmass Energy Frontier Simulations*, in *Proceedings, 2013 Community Summer Study on the Future of U.S. Particle Physics: Snowmass on the Mississippi (CSS2013): Minneapolis, MN, USA, July 29-August 6, 2013*, 2013. [1309.1057](#).
- [60] A. Avetisyan et al., *Methods and Results for Standard Model Event Generation at $\sqrt{s} = 14$ TeV, 33 TeV and 100 TeV Proton Colliders (A Snowmass Whitepaper)*, in *Proceedings, 2013 Community Summer Study on the Future of U.S. Particle Physics: Snowmass on the Mississippi (CSS2013): Minneapolis, MN, USA, July 29-August 6, 2013*, 2013. [1308.1636](#).
- [61] M. Cacciari, G. P. Salam and G. Soyez, *The Anti- k_t jet clustering algorithm*, *JHEP* **04** (2008) 063, [[0802.1189](#)].
- [62] M. Cacciari, G. P. Salam and G. Soyez, *FastJet User Manual*, *Eur. Phys. J. C* **72** (2012) 1896, [[1111.6097](#)].

- [63] G. Cowan, K. Cranmer, E. Gross and O. Vitells, *Asymptotic formulae for likelihood-based tests of new physics*, *Eur. Phys. J.* **C71** (2011) 1554, [[1007.1727](#)].
- [64] C. G. Lester and D. J. Summers, *Measuring masses of semiinvisibly decaying particles pair produced at hadron colliders*, *Phys. Lett.* **B463** (1999) 99–103, [[hep-ph/9906349](#)].
- [65] A. Barr, C. Lester and P. Stephens, *m_{T2} : The Truth behind the glamour*, *J. Phys.* **G29** (2003) 2343–2363, [[hep-ph/0304226](#)].
- [66] D. R. Tovey, *On measuring the masses of pair-produced semi-invisibly decaying particles at hadron colliders*, *JHEP* **0804** (2008) 034, [[0802.2879](#)].